CDK inhibition results in pharmacologic BRCAness increasing sensitivity to olaparib in BRCA1-WT and olaparib resistant in Triple Negative Breast Cancer

Esin Orhan, Carolina Velazquez, Imene Tabet, Lise Fenou, Geneviève Rodier, Béatrice Orsetti, William Jacot, Claude Sardet, Charles Theillet

CDK inhibition results in pharmacologic BRCAness increasing sensitivity to olaparib in BRCA1-WT and olaparib resistant in Triple Negative Breast Cancer

Esin Orhan[1] † , Carolina Velazquez[1] † , Imene Tabet[1], Lise Fenou[1], Geneviève Rodier[1], Béatrice Orsetti[1], William Jacot[1,2] https://orcid.org/0000-0001-7834-061X, Claude Sardet[1] https://orcid.org/0000-0001-7768-279X, Charles Theillet[1] https://orcid.org/0000-0001-5555-2759*

1. Institut de Recherche en Cancérologie de Montpellier, IRCM U1194, Montpellier University, INSERM, ICM, CNRS, Montpellier, France
2. Oncologie Clinique, Institut du Cancer de Montpellier, Montpellier, France

† equal contribution, * corresponding author, charles.theillet@inserm.fr, IRCM INSERM U1194, équipe Sardet, 208 avenue des Apothicaires, 34298 Montpellier cedex 5, France.

Running title : CDK9/12-inhibition impairs homologous-recombination and reverses olaparib-resistance

Keywords : BRCA1, TNBC, HRD, CDK9/12-inhibitor, pharmacologic-BRCAness.

Highlights:

- BRCA-deficient TNBC show increased PARPi sensitivity.
- Resistance associated with homologous recombination (HR) restoration is frequent.
- An HR impairing and BRCA-deficiency inducing pharmacologic approaches is of substance.
- Two CDK-inhibitors (CDKi), dinaciclib and SR-4835 were tested.
- CDKi impaired HR and increased olaparib sensitivity in TNBC cell lines and PDX models.

Abbreviations:

BRCA1-WT, BRCA1 wild type gene; BRCAness, BRCA-deficiency; CDK, Cyclin Dependent Kinase; CDKi, CDK inhibitors; CDDP, cisplatin; CTD, carboxy terminal domain; DSB, double strand DNA break; HRD, homologous recombination deficient or deficiency; IC50, median inhibitory concentration; PARPi, PARP inhibitor; PDX, patient derived tumor xenograft; TNBC, Triple Negative Breast Cancer.

Abstract:

One in three Triple Negative Breast Cancer (TNBC) is Homologous Recombination Deficient (HRD) and susceptible to respond to PARP inhibitor (PARPi), however, resistance resulting from functional HR restoration is frequent. Thus, pharmacologic approaches that induce HRD are of interest. We investigated the effectiveness of CDK-inhibition to induce HRD and increase PARPi sensitivity of TNBC cell lines and PDX models. Two CDK-inhibitors (CDKi), the broad range dinaciclib and the CDK12-specific SR-4835, strongly reduced the expression of key HR genes and impaired HR functionality, as illustrated by BRCA1 and RAD51 nuclear foci obliteration. Consequently, both CDKis showed synergism with olaparib, as well as with cisplatin and gemcitabine, in a range of TNBC cell lines and particularly in olaparib-resistant models. *In vivo* assays on PDX validated the efficacy of dinaciclib which increased the sensitivity to olaparib of 5/6 models, including two olaparib-resistant and one BRCA1-WT model. However, no olaparib response improvement was observed *in vivo* with SR-4835. These data support that the implementation of CDK-inhibitors could be effective to sensitize TNBC to olaparib as well as possibly to cisplatin or gemcitabine.

.

Introduction

BRCA1, BRCA2 and RAD51 proteins are central actors of homologous recombination (HR), which is the most accurate DNA double strand break (DSB) repair pathway (1). Patients with constitutional mutations in the *BRCA1* or *BRCA2* genes are prone to develop breast and ovarian cancer (2). Tumors that develop on BRCA-deficient background show Homologous Recombination Deficiency (HRD) and are characterized by elevated genetic instability and increased sensitivity to treatment, in particular to PARP-inhibitors (PARPi) or platinum salts (1),(3). The elevated sensitivity to treatment of BRCA-deficient cancers has long been associated with faulty DSB repair resulting from dysfunctional HR, but recent works have elegantly shown that the BRCA1, BRCA2 and RAD51 proteins play also important roles in the protection and repair of DNA replication forks (4),(5). Hence, increased genetic instability and accrued treatment sensitivity of BRCA-deficient tumors may result from the combination of faulty DSB repair and elevated levels of DNA replication stress.

HRD in breast and ovarian cancer has originally been associated with somatic mutations and epigenetic silencing of *BRCA1* and *BRCA2*, as well as, more recently, of *PALB2, RAD51B, RAD51C* or *RAD51D* which belong to the HR pathway (1). Interestingly, triple negative breast cancer (TNBC) and high grade ovarian cancers (HGOC) present the highest prevalence with respectively up to 35 and 50% of the tumors showing HRD (1),(2). Hence, innovative treatment protocols taking into account this HRD deficiency have been applied to these cancers. The central role of the PARP1 and PARP2 enzymes in DNA repair and particularly in HR have made PARPi molecules of choice on the basis of a synthetic lethal interaction between BRCA1/2 and PARP1 inactivation (6). As a matter of fact, PARPi have shown interesting results in treatment of BRCA-deficient ovarian cancers, as well as of breast cancers with constitutional *BRCA1* or *BRCA2* mutations (7),(8). However, BRCA-deficient models rapidly develop resistance to PARPi (9). Mechanisms leading to PARPi resistance in BRCA-deficient tumors frequently rely on complete or partial restoration of HR, either by the reactivation of a functional or hypomorphic BRCA1/2 variant or through the inactivation of the Shieldin complex due the loss of expression of either 53BP1, RIF1 or REV7 (10). Hence, despite their good initial response to treatment, BRCA-deficient cancer remains in need of a therapeutic approach that could reverse treatment resistance or reduce its occurrence. Ideally, such molecules should impact on the HR pathway and render it dysfunctional, thus, inducing a pharmacological BRCA-deficiency.

Among the different pathways considered, regulation by cyclin dependent kinases (CDKs) appeared of particular interest. CDKs belong to a large family of proteins broadly involved in either cell cycle or transcriptional regulation (11). In terms of functional impact on HR, CDK1 and CDK2 appear of interest. Indeed, in addition to their highly-documented role in cell cycle regulation, CDK1/2 also phosphorylate and regulate key actors of HR, such as BRCA1, BRCA2, PALB2 and CtIP (12). Furthermore, CDKs regulating transcription, such as CDK7, CDK9 and CDK12 have also attracted

attention as potential therapeutic targets in relation to HR. These CDKs phosphorylate specific serine residues of the C terminal domain (CTD) of the large subunit of RNApol II at different time points during transcription; CDK7 at initiation, CDK9 at early elongation, CDK12 at late stages of elongation and RNA processing (13). Their attenuation and/or pharmacological targeting have been proposed to reduce expression levels of principal HR genes and impact HR functionality (14). Noticeably, CDK12 has been proposed as playing a prominent role in the transcription and RNA processing of large genes belonging to DNA repair and HR (15),(16).

We, thus, evaluated whether attenuation/inhibition of CDKs could be an effective approach to impair the efficacy of HR and increase the sensitivity to treatment in triple negative breast cancer (TNBC) models. To this aim, we assessed the efficacy of two CDK inhibitors bearing different ranges of specificity. The first one, dinaciclib, is a broad range CDK-inhibitor, reported to target CDK1, CDK2, CDK5 and CDK9 and has more recently been proposed to target CDK12 (17). The second one, SR-4835 was specifically developed to target CDK12 and closely related CDK13 (18). Data presented in the present work show that treatment of TNBC cell lines with dinaciclib and SR-4835, both result in a sharp decrease of BRCA1 and RAD51 expression, as well as of BRCA1 and RAD51 nuclear foci formation upon genotoxic treatment, a marker of HR functionality (19), (20). Consistent with this broad impact on HR, dinaciclib and SR-4835 increased the sensitivity to cisplatin (CDDP), gemcitabine and to the PARPi olaparib of a series of TNBC models including BRCA-proficient, BRCA-deficient and importantly, also of olaparib-resistant cell lines. We, next, explored the efficacy of dinaciclib and SR-4835 in an *in vivo* setting using a set of TNBC and ovarian cancer PDX models, of which we had determined the response to olaparib (20). Noticeably, dinaciclib showed remarkable efficacy and improved the response to olaparib in most PDX tested, including two olaparib resistant and one BRCA1-WT model, resulting in an improved response associated with a strong reduction of the BRCA1 and RAD51 nuclear foci. On the other hand, SR-4835, while showing an *in vitro* efficacy equivalent to that of dinaciclib, produced no improvement of the olaparib response in any of the PDX models tested.

Overall, these data support that the implementation of CDKi, in particular dinaciclib, could be an effective approach to sensitize TNBC to olaparib and suggest that they could also be advantageous used in combination with cisplatin or gemcitabine.

Materials and Methods

Cell lines and CRISPR-Cas9 engineered mutants.

SUM159PT and SUM149PT TNBC cell lines a generous gift from Dr S Ethier (MUSC, Charleston, SC), were maintained in Ham's F-12 medium (Gibco™, Fisher Scientific, Illkirch-Graffenstaden, France) supplemented with 5% FBS, 10µg/ml insulin, 1µg/ml hydrocortisone and 1% antibiotic-antimycotic (100X) (Gibco™, Fisher Scientific, Illkirch-Graffenstaden, France). UWB1.289PT cell line was obtained from the American Type Culture Collection (ATCC) and maintained in the 50% RPMI-1640 (Gibco™), 50% MEGM (MEGM Bullet Kit; CC-3150, Lonza, Basel, Switzerland) and supplemented with 3% FBS, 1% Antibiotic-antimycotic (100X) (Gibco™, Fisher Scientific, Illkirch-Graffenstaden, France). For CRISPR-Cas9 KO clone generation, SUM159PT cells were first transduced with a plasmid vector containing doxycycline inducible lentiviral expression of SpCas9 (pCW-Cas9, #50661, Addgene). Lentiviral transduction was performed on 70% confluent cell cultures. Viral particles were added in the fresh medium containing 8µg/ml polybrene. After 16h the medium was changed and 2µg/ml puromycin added for a 5day selection. Next, cells were transduced with two lentiviral plasmid vectors expressing sgBRCA1 (kind gift from Yea-Lih Lin, IGH, Montpellier) and selected with 400µg/ml G418 for 10 days or with RAD51C or RAD51D gRNAs (Synthego Corp. Redwood City, CA. USA). Cas9 expression was induced by adding 1µg/ml of doxycycline for 6 days. Next, clones were obtained by limit dilution of the cells and then analyzed by Sanger sequencing and western blotting to isolate BRCA1 knock out clones. All cell lines and selected clones were genetically typed by Eurofins Genomics cell line authentication (Eurofins Genomics, Les Ulis, France).

Cell viability tests

The median inhibitory concentration (IC50) was determined for each individual compound or drug combination using the cell counting kit-8 (CCK-8, Tebubio, Houdan, France), in which cell viability is measured with a colorimetric assay based on the reduction by cellular dehydrogenases of the water-soluble tetrazolium salt (WST-8) which is transformed in formazan (yellow). The level of yellow dye, which is directly proportional to the number of living cells, was measured by colorimetry at 540nm using the Pherastar instrument (BMG labtek) microplate reader. In short, 1500 cells were seeded onto 96-well flat-bottom plates on day 1. On day 2 cells were exposed for 24 h to increasing concentrations of the tested drugs. The medium was then replaced and cells were grown for 2 doubling times at 37°C and 10µl of CCK-8 were added to each well. Average +/- standard deviation values of three independent experiments were plotted using GraphPad Prism software.

Determination of drug synergism

About 1500 cells were seeded in individual 96 flat-bottom well plates and once attached combination treatments were tested in a matrix configuration at growing concentrations (drug 1 in

the X axis and drug 2 in the Y axis). Cells were exposed to the drugs for 24 h after which cell viability was determined as described in cell viability tests. Synergism was determined as previously described (23).

Flow cytometry determination of cell cycle changes and cell mortality upon treatment

Approximately $1x10^6$ cells were grown for 24 h in 10 cm Petri dishes and subjected to olaparib, dinaciclib, olaparib+dinaciclib, SR-4835 or olaparib+SR-4835 treatment for 24 h. After 24 h, drugs were removed and fresh medium added. Cell aliquots were collected at time points 0h, 24 h, 48 h and 72 h. At each time point, cells were washed once with icecold PBS, trypsinized and counted. Cells were fixed in ice-cold 70% ethanol, washed in ice-cold PBS before being suspended in 0.5 ml staining solution and stored at -20°C until analysis. For cell cycle analysis, DNA was counterstained with 1µg/ml DAPI and cells incubated at RT for 30min. FACS analysis was performed using a Gallios Flow instrument (Beckman Coulter, Villepinte, France). DNA fluorescence was collected in linear mode, cell debris and doublets were excluded. Settings were identical in each channel and 10 000 cells were analyzed per aliquot. Each experiment was performed three times. Quantification of cell death was done on cell pellets rinsed once in cold PBS and a second time in cold BBA buffer (sterile 0.2mM HEPES pH7.4, 1.4M NaCl, 25mM CaCl2). Cells were distributed and resuspended in 50µl BBA buffer + 1µl annexinV (#11828681001 Sigma Aldrich) and 1µg/ml propidium iodide (PI) and incubated at RT for 30min. Then 200µl PBS were added and cells analyzed.

Protein extraction and western blotting

Protein extracts were prepared by lysing either tumor tissue or cell line pellets on ice for 30 min in 50mM Tris-HCl pH7.4, 100mM NaCl, 50mM NaF, 40mM β-glycerophosphate, 5mM EDTA, 1% Triton X100, 1µM aprotinin, PMSF, 1µM leupeptin, 1µM pepstatin, followed by a short centrifugation to pellet debris. Protein concentrations were measured using the BCA kit (#23221, Pierce). SDS-PAGE gel electrophoresis was carried out on 30µg protein in 6.5% and 7.5% for <200kDa and > 200 kDa proteins respectively. Subsequently proteins were transferred onto nitrocellulose membranes (#1030000, Amersham), incubated overnight at 4°C with the primary antibody. Antibodies used are listed in a separate section. Membranes were then washed and incubated with the appropriate secondary antibody in 5% non-fat dry milk in TBST (20mM Tris-HCl pH7.4, 150mM NaCl, 0.1% Tween20) for 2H at room temperature and revealed by incubation with Chemiluminescent HRP Substrate (#WBKLS0500, Millipore).

Immunofluorescence

For cell lines, cells were grown on 12mm diameter slides coverslips in 24 well-plate for 24 h and drugs were added at the predetermined IC50 concentration. After 24 h drugs were washed off and cells prepared. For tumor tissues, 6µm cryosections were prepared from OCT embedded deep frozen tissue

and mounted on Fisherbrand™ Superfrost™ Plus Microscope Slides (Fisher Scientific, Illkirch-Graffenstaden, France) and stored at -80°C until use. Cells and tumor sections were sequentially subjected to mild extraction 5min in cold PBS containing 0.4% Triton X100, fixed in in PBS containing 4% PFA. Blockage/permeabilization was performed for 1 h at RT in 3% BSA and 0.2% Triton X100 diluted in PBS (solution 1). Next the primary antibody was diluted in solution 1 and incubated overnight at 4°C, after which the secondary antibody in solution 1 was incubated at room temperature for 1 h. Between each step, slides were washed 3 times with PBS. Tumor cryosections were immersed in 0.1% SBB (Sigma Aldrich, Saint Quentin Fallavier, France) and 70% ethanol for 20 min at room temperature to reduce tissue autofluorescence and subsequently washed three times for 5 minutes in PBS with 0.02% Tween 20. DNA was counterstained with 1µg/ml DAPI (Fisher Scientific, Illkirch-Graffenstaden, France) to stain the nuclei and coverslips were mounted with MWL4-88 Citifluor (#17977-150 CliniSciences, Nanterre, France) and stored at 4°C. Antibodies used are described in the Antibody section. Immunofluorescence images were acquired using Zeiss AXIO Imager.M2 microscope using a 63X-immersion oil lens and generated using Zeiss Blue software. Cells with ≥5 foci in the nucleus were scored using CellProfiler (version 2.2.0, Broad Institute), as described (19), (20). At least three biological replicates (both vehicle- and olaparib-treated) were analyzed.

Antibodies

Immunofluorescence; rabbit anti-RAD51 PC130 1:300 (Merck Millipore Sigma Aldrich, Saint Quentin Fallavier, France,), rabbit anti-geminin 52508 1:200 (Cell Signaling Technology, OZYME, Saint Cyr l'Ecole, France), mouse anti-BRCA1 sc-6954 1:100 (Santa Cruz Biotechnology, Heidelberg, Germany), mouse anti-γ-H2AX 1:4000 (H2-3F4, kind gift from Dr. Mustapha Oulad-Abdelghani, MAB-IGBMC Illkirch-Graffenstaden), rabbit anti-53BP1 NB100-304 1:500 (Bio-technee LTD, Abington, UK). Secondary antibodies; goat anti-mouse Alexa Fluor 488 (Abcam ab150113, 1:1000), goat anti-rabbit Alexa Fluor 555 ab150078 1:1000 (Abcam, Cambridge, UK).

Western blotting; BRCA1 9010 1:500 (Cell Signaling Technology OZYME, Saint Cyr l'Ecole, France), BRCA2 A303-434A 1:1000 (Bethyl OZYME, Saint Cyr l'Ecole, France), PARP1 WH0000142M1 1:1000 (Sigma Aldrich, Saint Quentin Fallavier, France), RAD51 8875, 1:1000 (Cell Signaling Technology OZYME, Saint Cyr l'Ecole, France) and alfa tubulin T9026 1:20000 (Sigma Aldrich, Saint Quentin Fallavier, France); secondary antibodies goat anti-mouse-HRP 70745 1:10000 (Cell Signaling Technology OZYME, Saint Cyr l'Ecole, France) and goat anti-rabbit-HRP 7076 1:10000 (Cell Signaling Technology OZYME, Saint Cyr l'Ecole, France).

TNBC and HGSOC PDX models and in vivo treatment

TNBC and Ovarian cancer PDX models establishment was as described (21), (22). PDX models are described in Table 2. The study was reviewed and approved by the ethics committees for animal

experimentations of the University of Montpellier (CEEA-LR-12028). PDX models were established from fresh tumor fragments obtained from the Pathology Department at the Comprehensive Cancer Center of Montpellier (ICM) after informed consent of the patients. Establishment of PDX models was reviewed and approved by the institutional review board. Approximately 50 mm3 PDX fragments were grafted subcutaneously into the flank of 3-4 week old Swiss-nude female mice (Charles Rivers, Saint-Germain-sur-l'Arbresle, France). The present study comprised six experimental arms; vehicle, olaparib, dinaciclib, olaparib + dinaciclib, SR-4835 and olaparib + SR-4835 each comprising 8 mice. When median tumor volume reached 100-150 mm3, mice were randomly distributed in the six arms and treatment was started. Olaparib (Lynparza, AstraZeneca) was administered orally 5 times/week for 5 weeks at 100 mg/kg. Dinaciclib (Accord Healthcare, Middlesex, UK) was administered by intra-peritoneal (IP) injection twice per week for 5 weeks at 30mg/kg, SR-4835 (MedChemExpress, #HY-130250, Monmouth Junction, NJ 08852, USA) was administered orally twice a week at 30 mg/kg for 5 weeks. Complementary tests were made in which SR-4835 was injected IP at 30 mg/kg twice a week for 5 weeks. At treatment end, mice were euthanized to collect tumor samples for further biochemical (RNA and proteins) or histological analyses.

Transcriptome analysis

Expression profiling was performed on Affymetrix Human Genome GeneChip HG133Plus at the MGX-transcriptome platform (BioCampus-IRMB) according to the manufacturer's recommendation. Raw feature data were normalized using Robust Multi-array Average (RMA) method (R package affy). between drug-treated cells paired with DMSO-treated cells were identified using the differential gene expression analysis method (R Package"DESeq2"). Differentially expressed genes were ranked by their p-value. Differentially expressed genes were annotated with GSEA using Hallmark gene set (www.gsea-msigdb.org/gsea/index.jsp).

RT qPCR

Total RNA was isolated from cell lines lysed in TRIzol (Invitrogen, Fisher Scientific, Illkirch-Graffenstaden, France), while PDX tumors were lysed using Lysing Matrix D (MP Biomedicals™, Doornveld, France). Subsequently, the RNA was extracted using the RNeasy Kit (Qiagen, Les Ulis, France) following manufacturer instructions. cDNAs were synthesized from 1µg of total RNAs using random hexamers and SuperScript III Reverse transcription (Invitrogen, Fisher Scientific, Illkirch-Graffenstaden, France). Real-time qPCR was performed on a LightCycler 480 SW 1.5 apparatus (Roche, Meylan, France) with ONEGreen® FAST QPCR PREMIX (Ozyme, Saint Cyr l'Ecole, France) and designed human specific primers (Table 1). Results were quantified with a standard curve generated by serial dilutions of a reference cDNA preparation. GAPDH transcripts were used for normalization. The fold change in gene expression was calculated as: Fold change = $2^{-\Delta\Delta CT}$.

Statistical analysis

Data expressed as mean values +/- SD of three independent experiments were analyzed using GraphPad Prism version 8.1 for Windows (GraphPad Software, Boston, Massachusetts USA) using a two-tailed unpaired Student t test. In vivo tumor growth data were analyzed according to non-linear quadric fit model using the equation of Y=100*exp(-1*(A*X + B*X^2)) on GraphPad Prism version 8.1 (GraphPad Software, Boston, Massachusetts USA).

Results

CDK-inhibitors, dinaciclib and SR-4835, synergistically increase the efficacy of olaparib

The median inhibitory concentrations (IC50) for olaparib, CDDP, gemcitabine, dinaciclib and SR-4835 were determined in a set of 13 TNBC and 5 ovarian cancer cell lines comprising 5 BRCA1-WT, 9 BRCA1-deficient or HRD-deficient (RAD51C and RAD51D KO) and 5 BRCA1-deficient models selected for olaparib resistance using the cell counting kit-8 (CCK-8) assay that measures cell viability (Supplementary Figure 1A). IC50 determination resulted from 12 replicated experiments (3 biological replicates and 4 technical replicates). As expected, BRCA1-deficient cell models were the most sensitive to olaparib. Moreover, we noted that BRCA1-deficient cell lines were more sensitive to dinaciclib in comparison with their olaparib resistant counterparts. Other tested drugs did not show statistically significant differences in sensitivity according to their BRCA status (Figure 1A).

Next, using two-drug combinations and viability tests, we assessed the existence of synergistic interactions between olaparib and dinaciclib or olaparib and SR-4835. The two drug combinations to be tested, olaparib+dinaciclib (ola+dina) or olaparib+SR-4835 (ola+SR), were distributed in a matrix configuration at growing concentrations and cell viability was determined. Three TNBC cell lines, two BRCA1-WT (BT549 and SUM159) and one BRCA1-null (MDA-MB-436) were used as models and synergism was computed as described (23) (Figure 1B-C). Remarkably, both dinaciclib and SR-4835 used at concentrations ranging 0.5 to 15nM (Figure 1B-C) showed synergy with olaparib in the 3 cell lines. Next, in combination with olaparib, we introduced dinaciclib or SR-4835 at fixed concentrations (1nM or 10nM) to assess if this was associated with a significant reduction in IC50 concentrations of olaparib. Noticeably, dinaciclib and SR-4835 at 1 or 10nM induced a 10 to 100-fold sensitivity increase in the cell lines tested (Figure 1D). However, this sensitivity increase varied according to the cell line, being most potent on models that had acquired resistance to olaparib and least effective in olaparib sensitive BRCA1-deficient models (Supplementary Figure 1B). We also assessed and compared the impact of these combinations on cell mortality of dinaciclib or SR-4835 introduced in combination with olaparib in the *BRCA1*-WT SUM159B1 cell line and its isogenic BRCA1-deficient SUM159B1KO cells, we engineered from SUM159B1 cells by CRISPR. Remarkably, in comparison with olaparib used as a single drug, both ola+dina and ola+SR combinations increased up to 4fold the

mortality in the BRCA-proficient SUM159B1 cells (Figure 1E). However, in the BRCA1-KO SUM159B1KO cells, which expectedly showed superior sensitivity to olaparib, the potentiating effect of dina and SR was more modest, increasing the short term mortality at 24 h of drug exposure, but showing no advantage over olaparib alone at 72 h (Figure 1F).

Dinaciclib and SR-4835 downregulate HR gene expression and impede HR functionality

Dinaciclib and SR-4835 have both been reported to induce concentration-dependent reduction of the phosphorylation at the Serine 2 residue of the RNA pol II CTD domain, resulting in downregulated expression of a wide range of genes including those belonging to the HR pathway (17), (18). Here, we analyzed gene expression changes induced in SUM159B1. Whole genome Affymettrix RNA profiling showed that both dinaciclib and SR-4835 strongly impinged on cell cycle regulation and checkpoints and DNA repair pathways (Supplementary Figure 2A, B). To confirm the impact of these drugs on DNA repair genes, we next monitored by RT-QPCR the mRNA levels of 8 selected genes in BRCA1-WT SUM159B1 cells exposed for 24h exposure to 10nM of either dinaciclib or SR-4835. While ola+SR treatment resulted in a 3 to 30fold reduction of mRNA expression for the 8 genes, ola+ dina treated cells showed a strong reduction only for *BRCA1, BRCA2, ATR* and *ATM* mRNA expression (Figure 2A). At the protein level, however, ola+ dina and ola+SR treated cells displayed similar reduced protein expression for BRCA1, BRCA2 and RAD51, which appeared obliterated (Figure 2B). Surprisingly, while *ATM* and *ATR* mRNA expression levels were strongly decreased upon CDKi treatment, no apparent reduction was observed at the protein level at the time point analyzed, possibly resulting from different protein half-lives.

Because the capacity of a tumor to form BRCA1 and RAD51 nuclear foci is an accepted readout of HR functionality, we assessed the number of foci-positive cells in olaparib-treated SUM159B1, in comparison with SUM159B1 treated with ola+dina or ola+SR (19), (20). In accordance with the decreased BRCA1 and RAD51 abundance, the number of BRCA1 and RAD51 foci positive SUM159B1 cells was severely reduced by ola+dina and ola+SR treatment (Figure 2C, D, E). Importantly, cells treated with either dinaciclib or SR-4835 alone showed no increase in BRCA1 or RAD51 foci numbers (Figure 2D, E). However, we noted that BRCA2 and FANCD2 nuclear foci, two key HR or DDR actors, were also severely reduced in ola+dina and ola+SR treated cells (Supplementary Figure 3A, B). This suggested that both dinaciclib and SR-4835 had the potency to impair HR and the DDR response.

We were interested to test which of the genetic attenuation of CDK9, CDK12 or CDK13, by means of siRNA, phenocopied best the effect of dinaciclib and SR-4835 on BRCA1 and RAD51 foci formation in presence of olaparib. Interestingly, both CDK9 and CDK12 attenuation resulted in the reduction of BRCA1 and RAD51 foci with equivalent efficacy (Figure 2H). However, we were intrigued to see that CDK13 attenuation strongly reduced RAD51 foci, while it appeared to have no or little impact on BRCA1 foci formation (Figure 2H, I).

However, HR functionality being strictly restricted to S and G2 cell cycle phases, it was important to verify whether dinaciclib or SR-4835 treated cells were not depleted in S phase cells, thus, explaining reduced BRCA1 and RAD51 nuclear foci. The FACS cell cycle analysis did not reveal any G1 block nor major shift in cell cycle distribution when we compared olaparib with ola+dina or ola+SR treated cells (Supplementary Figure 3C).

Dinaciclib and SR-4835 revert HR restoration and reinstate sensitivity in olaparib-resistant cell models

Emergence of olaparib resistance (ola-res) in BRCA-deficient models is frequently associated with restoration of HR proficiency (10). We selected 3 ola-res models from 3 BRCA1-deficient cell lines by cultivating them with gradually increased olaparib concentrations (20). The parental BRCA1-deficient cell lines corresponded to SUM159B1KO, SUM149PT which bear a frameshift mutation in exon 11 (2288delT) and UWB1.289PT ovarian cancer cells also mutated in exon 11 (2594delC). Parental cells either did not express the BRCA1 protein or expressed a 100kD form corresponding to the hypomorphic δ11-BRCA1 variant (Supplementary Figure 4) (24). Noticeably, ola-res daughter cells reexpressed at various levels the full length BRCA1 protein (SUM159B1BO-Re and SUM149-ola-Re) or showed a strong overexpression the δ11-BRCA1 variant (UWB.289-ola-Re) suggesting restored HR functionality (Supplementary Figure 4). In coherence with a reinstatement of HR competence in the three ola-res clones, these cells presented restored capacities of BRCA1 and RAD51 foci formation upon olaparib treatment, in comparison with their BRCA1-deficient parental cells (Figure 3). Noticeably, the restored capacity to form BRCA1 and RAD51 foci observed in ola-res cells was obliterated by ola+dina or ola+SR treatment (Figure 3). These results were in coherence with the strong reduction of olaparib IC50 concentrations observed in these ola-res models treated with dinaciclib or SR-4835 combinations indicating that both CDKi were able to revert the functional restoration of HR in these models and reinstate their sensitivity to olaparib (Figure 1D).

Overall, these data suggested that combination treatments based on dinaciclib or SR-4835 could be a solution to induce pharmacological BRCAness and increase treatment sensitivity in TNBC.

Dinaciclib significantly increased the olaparib response of PDX models.

Our next step aimed at validating the *in vitro* observations made on cell line models in a preclinical *in vivo* setting. To this aim, we selected 6 PDX models (5 TNBC and one High Grade Ovarian Carcinoma), characterized in a previous work (20), of which we determined the sensitivity to olaparib (Table 2). The six PDX bore different BRCA1 profiles; 2 were *BRCA1*-WT (b3804, b1995), 3 bore a promoter hypermethylation that silenced the *BRCA1* gene (b3977, 15b0018, b4122), while the last model (o10047) displayed a large deletion in the *BRCA1* gene spanning exons 8 through 13 (20). PDX were grafted subcutaneously onto 8 Swiss-nude mice per experimental group and tumor volumes were monitored twice per week in the 6 experimental groups tested over the duration of the assay. Mice in group 1 received the vehicle, in group 2 they were administered 100 mg/kg olaparib orally

5days/week for 5 weeks, in group 3 two intraperitoneal (IP) injections of 30 mg/kg dinaciclib per week for 5 weeks, in group 4 five oral administrations per week of 100mg/kg olaparib and two (IP) injections of 30 mg/kg dinaciclib per week for 5 weeks, group 5 two oral administration of 30 mg/kg of SR-4835 twice a week for 5 weeks, group 6 five oral administrations per week of 100mg/kg olaparib and two oral administration of 30 mg/kg per week of SR-4835 for 5 weeks.

As shown in Figure 4A and Supplementary Figure 5, four of six PDXs progressed under olaparib (b3804, b1995, b3977, 15b0018), while two models showed either stabilized growth (b4122) or tumor regression (o10047). It was of note that, under ola + dina treatment, five of six PDX models either regressed (b4122, o10047) or showed stabilized growth (b1995, b3977, 15b0018) (Figure 4A, Supplementary Figure 5). On the other hand, PDX b3804 progressed both under olaparib and in ola +dina treated mice, albeit at a slightly reduced pace (Supplementary Figure 5). However, in group 6 (ola + SR) all PDX models progressed under treatment (Supplementary Figure 6). These data led us to withhold further *in vivo* work with SR-4835 and to re-focus our investigation on dinaciclib only.

We also tested the impact of ola + dina treatment on BRCA1 and RAD51 nuclear foci formation *in vivo*. BRCA1 and RAD51 immunofluorescence labeling was performed on 5 µm sections of PDX tumors collected within 24h after the last drug administration (Figure 4B). As expected tumors issued from olaparib-treated PDXs showed strongly increased BRCA1 and RAD51 foci-positive cell numbers (except PDX b4122 which was clearly BRCA-deficient). Consistently with our *in vitro* observations, PDX tumors from ola + dina treated models all showed severely reduced foci formation in comparison with tumors treated with olaparib alone (Figure 4C, D). These data, thus, indicated the *in vivo* potency of dinaciclib, as it induced HR impairment, even in a BRCA1-WT context, and resulted in increased responsiveness to olaparib in 5/6 PDX models tested in this work.

Discussion

BRCA-deficient tumors, as a consequence of homologous recombination deficiency (HRD), show improved response to PARPi or platinum salts (1). However, these tumors invariably develop resistance to treatment, which, in a sizeable fraction of cases, is associated with partial or complete functional restoration of HR, hence emphasizing the need of pharmacologic approaches to induce BRCA-deficiency (9), (10). A number of pathways impinging on the functionality of the BRCA-pathway are being explored in search of effective inhibitors (25). Among these cyclin dependent kinases (CDKs) are of particular interest.

CDKs form a family of 20 serine/threonine kinases that regulate cell cycle progression and proliferation at different levels (11). Noticeably, a subset of CDKs have been shown to impact on DNA repair and homologous recombination (HR) pathways. Indeed, CDK1 and/or CDK2 have been shown to phosphorylate and activate BRCA1, BRCA2, PALB2 and CtIP (26),(12), while CDK9 and CDK12 have been proposed to regulate mRNA expression of key HR genes (27). Genetic attenuation of *CDK12* has been shown to result in downregulated expression of large size genes including *BRCA1*, *BRCA2* or *ATM* (17),(18). Furthermore, *CDK12* inactivation has been associated with impaired DNA repair gene expression in ovarian cancer (28) and its identification in a genome wide screen for synthetic lethal interactions with PARP1/2 inhibition reinforced its status as a therapeutic target of choice (29). The CDK12 and CDK9 proteins share extensive structural similarities, especially at proximity of the ATP binding site. This led to show that CDK9 inhibitors, such as flavopiridol or dinaciclib, were also active against CDK12 (17). Furthermore, some authors suggested that CDK9 attenuation, despite having a wider impact on gene expression than CDK12, may also result in reduced DNA repair gene expression (30). The siRNA attenuation data presented in this work clearly confirmed the impact of CDK12 downregulation on HR functionality, but also showed that CDK9 attenuation had a sizeable impact. This suggested that targeting CDK9 concomitantly to CDK12 could be of benefit compared with CDK12 alone.

In this work, we aimed at comparing the relative efficacies in terms of HR impairment and induction of BRCA-deficiency of two CDK inhibitors (CDKis) bearing different ranges of specificities; dinaciclib and SR-4835. Dinaciclib was shown to target CDK1, CDK2, CDK5, CDK9 in a 3 to 12nM range, as well as CDK12 at 50nM (31), whereas SR-4835 inhibits CDK12 and CDK13 in the 10 to 100nM range and has little reported activity against CDK1, CDK2 or CDK9 (18). Our data indicated that both inhibitors induced HR deficiency with similar potencies on cultured cell models. Indeed, dinaciclib as well as SR-4835 treatment induced an important reduction of mRNA and protein expression levels of key HR actors such as *BRCA1*, *BRCA2*, *PALB2* or *RAD51*. Their negative impact on BRCA-proficiency was further confirmed by the strongly reduced capacity to form nuclear BRCA1, BRCA2, RAD51 and FANCD2 foci in dinaciclib and SR-4835 treated models. Overall, dinaciclib and SR-4835 also disrupted

these markers of HR functionality with equivalent efficacy in cell lines with acquired olaparib resistance, indicating that both CDKis may be therapeutic tools of interest. In line with their capacity to induce BRCA-deficiency, both dinaciclib and SR-4835 interacted synergistically with olaparib in a number of the cell models tested here, allowing to reduce olaparib concentrations up to 1000fold. Interestingly, we performed a pilot investivation which showed similar concentration reductions when we combined dinaciclib or SR-4835 with cisplatin or gemcitabine, thus indicating that synergism could be extended to other drugs beyond olaparib (Supplementary Figure 7). Noticeably, however, the relative synergistic efficacy of dinaciclib or SR-4835 varied substantially according to the cell model, suggesting it could be affected by tumor-specific genetic or epigenetic background. Interestingly, tested *in vivo* on PDX models, dinaciclib showed remarkable efficacy and, thus, validated *in vitro* observations. Indeed, five of six PDX treated with dinaciclib + olaparib showed a clearly improved response compared with models treated with olaparib alone. This was noted in two BRCA1-deficient models in which response was improved by 50 to 70%, as well as in one olaparib non-responsive BRCA1-WT and two olaparib-resistant BRCA1-deficient PDXs. Furthermore, in olaparib + dinaciclib treated PDXs BRCA1 and RAD51 foci formation was obliterated, indicating the impact of dinaciclib on HR functionality in an *in vivo* context. The anti-tumor efficacy of dinaciclib has been studied in diverse cancer types either as a single agent or in various combinations. As a single agent, it has shown limited impact on tumor growth despite its association with significant downregulation of *MYC* and *CCND1* expression, as well as a strong reduction of CDK1 and RB phosphorylation (32,33) (34,35). Interestingly, dinaciclib-treated tumors displayed increased immunogenicity due to accrued neoantigen presentation and showed a clear synergism with anti-PD1 treatment (36). Hence, in addition to improving the tumor response to PARPi or platinum salts, dinaciclib could be an interesting lever to improve the anti-tumor immune response. Furthermore, dinaciclib is reported in 18 ongoing clinical trials, among which one in combination with the PARPi veliparib (NCI-2011-03458) showing that the combination treatment was well tolerated by patients and showed limited anti-tumor activity in non-BRCA1 carriers. However, dinaciclib was administered twice during the course of the treatment and the half-life of dinaciclib may be too short for this regimen (37). On the other hand, our SR-4835 *in vivo* results did not match expectations raised by *in vitro* observations. Indeed, no improvement in terms of tumor growth was seen in any of the four PDX models treated with SR-4835, either in single drug administration or in combination with olaparib. As SR-4835 was administered orally at 30mg/kg, we wondered whether insufficient stability may have limited the efficacy of the drug. As a potential alternative, we tested intraperitoneal injection of SR-4835 on two PDX models, which did not show any apparent benefit, presented multiples signs of renal and hepatic toxicity. Our data, thus, suggest that despite its proven efficacy *in vitro,* the modest potency of SR-4835 *in vivo* may be related to limited bioavailability.

In conclusion, the data presented here strongly support the great potential of CDK9 and/or CDK12 inhibitors, in terms of pharmacologic BRCAness induction. Indeed, both dinaciclib and SR-4835 impacted HR functionality as illustrated by the clear reduction of BRCA1 and RAD51 foci formation in treated cell models that was associated with the reversion of olaparib resistance in cell models. The fact that dinaciclib potently induced HR deficiency at nanomolar concentrations in BRCA1-proficient or olaparib resistant PDX strongly suggest that it could be of interest in the clinic to induce pharmacologic BRCAness and prevent or delay emergence of PARPi resistance (17). It is of note that dinaciclib has been FDA approved and could, thus, be the subject of clinical trials adjusted at patients with BRCA-deficient breast or ovarian tumors who recurred after a PARPi first line treatment.

Conflict of interest:

None of the authors has a conflict of interest to disclose

Author contribution

Esin Orhan, Carolina Velazquez, Imene Tabet; investigation, drafting, methodology. Lise Fenou, Geneviève Rodier; investigation and methodology. Beatrice Orsetti; Resources. William Jacot, Claude Sardet; investigation, validation, drafting, funding. Charles Theillet; Conceptualization, validation, Funding acquisition, drafting and writing the manuscript.

Ethics approval

Patients whose tumor was used to generate PDX signed informed consent and the preclinical assay was reviewed and approved by the ethics committees for animal experimentations of the University of Montpellier (CEEA-LR-12028) and received the approval number 25612.

Data availability

Expression profiling data deposit on Geo database is currently

Acknowledgements

The authors sincerely acknowledge Dr Isabelle Jariel for critical reading and constructive comments on the manuscript, Dr Stanislas du Manoir and late Dr Rui-Bras Gonçalvez for help during the establishment of the PDX models. Furthermore, sincere thanks are due to the staffs of the animal facility at IRCM and the Centre de Ressources Biologiques at ICM for their constant support and expert help.

Funding information

This work benefited from the following financial support: Astra-Zeneca contract # 2018-02069, Institut National du Cancer PRTK-2017 MODUREPOIS, Ligue Nationale Contre le Cancer 'Comité régional Occitanie-Est' 2021-R22031FF and the SIRIC Montpellier Cancer Grant INCa-DGOS-Inserm_12553.

Author information

Carolina Velazquez, present address; Gynecological Oncology Laboratory, Department of Oncology, KU Leuven and Leuven Cancer Institute (LKI), 3000 Leuven, Belgium.

References

1. Lord CJ, Ashworth A. BRCAness revisited. Nature Publishing Group. 2016 Feb;16(2):110–20.

2. Couch FJ, Hart SN, Sharma P, Toland AE, Wang X, Miron P, et al. Inherited Mutations in 17 Breast Cancer Susceptibility Genes Among a Large Triple-Negative Breast Cancer Cohort Unselected for Family History of Breast Cancer. Journal of Clinical Oncology. 2015 Jan 29;33(4):304–11.

3. Konstantinopoulos PA, Ceccaldi R, Shapiro GI, D'Andrea AD. Homologous Recombination Deficiency: Exploiting the Fundamental Vulnerability of Ovarian Cancer. Cancer Discovery. 2015 Nov 1;5(11):1137–54.

4. Quinet A, Tirman S, Jackson J, Šviković S, Lemaçon D, Carvajal-Maldonado D, et al. PRIMPOL-Mediated Adaptive Response Suppresses Replication Fork Reversal in BRCA-Deficient Cells. Molecular Cell. 2020 Feb 6;77(3):461–9.

5. Vugic D, Dumoulin I, Martin C, Minello A, Alvaro-Aranda L, Gomez-Escudero J, et al. Replication gap suppression depends on the double-strand DNA binding activity of BRCA2. Springer US; 2023 Jan 27;:1–19.

6. Turner NC, Lord CJ, Iorns E, Brough R, Swift S, Elliott R, et al. A synthetic lethal siRNA screen identifying genes mediating sensitivity to a PARP inhibitor. EMBO J. 2008 May 7;27(9):1368–77.

7. Drew Y, Mulligan EA, Vong WT, Thomas HD, Kahn S, Kyle S, et al. Therapeutic Potential of Poly(ADP-ribose) Polymerase Inhibitor AG014699 in Human Cancers With Mutated or Methylated BRCA1 or BRCA2. JNCI Journal of the National Cancer Institute. 2011 Feb 15;103(4):334–46.

8. Chopra N, Tovey H, Pearson A, Cutts R, Toms C, Proszek P, et al. Homologous recombination DNA repair deficiency and PARP inhibition activity in primary triple negative breast cancer. Nat Comms. 2020 May 29;11(1):2662.

9. D'Andrea AD. Mechanisms of PARP inhibitor sensitivity and resistance. DNA Repair. 2018 Nov;71:172–6.

10. Brugge ter P, Kristel P, van der Burg E, Boon U, de Maaker M, Lips E, et al. Mechanisms of Therapy Resistance in Patient-Derived Xenograft Models of BRCA1-Deficient Breast Cancer. JNCI Journal of the National Cancer Institute. 2016 Nov;108(11).

11. Malumbres M. Cyclin-dependent kinases. Genome Biol. 2014;15(6):122.

12. Diril MK, Ratnacaram CK, Padmakumar VC, Du T, Wasser M, Coppola V, et al. Cyclin-dependent kinase 1 (Cdk1) is essential for cell division and suppression of DNA re-replication but not for liver regeneration. Proceedings of the National Academy of Sciences. 2012 Mar 6;109(10):3826–31.

13. Harlen KM, Churchman LS. The code and beyond: transcription regulation by the RNA polymerase II carboxy-terminal domain. Nat Rev Mol Cell Biol. 2017 Apr;18(4):263–73.

14. Blazek D, Kohoutek J, Bartholomeeusen K, Johansen E, Hulinkova P, Luo Z, et al. The Cyclin K/Cdk12 complex maintains genomic stability via regulation of expression of DNA damage response genes. Genes & Development. 2011 Oct 19;25(20):2158–72.

15. Dubbury SJ, Boutz PL, Sharp PA. CDK12 regulates DNA repair genes by suppressing intronic polyadenylation. Nature. 2018 Dec;564(7734):141–5.

16. Chirackal Manavalan AP, Pilarova K, Kluge M, Bartholomeeusen K, Rajecky M, Oppelt J, et al. CDK12 controls G1/S progression by regulating RNAPII processivity at core DNA replication genes. EMBO Rep. 2019 Sep;20(9):e47592.

17. Johnson SF, Cruz C, Greifenberg AK, Dust S, Stover DG, Chi D, et al. CDK12 Inhibition Reverses De Novo and Acquired PARP Inhibitor Resistance in BRCA Wild-Type and Mutated Models of Triple-Negative Breast Cancer. CellReports. ElsevierCompany; 2016 Nov 22;17(9):2367–81.

18. Quereda V, Bayle S, Vena F, Frydman SM, Monastyrskyi A, Roush WR, et al. Therapeutic Targeting of CDK12/CDK13 in Triple-Negative Breast Cancer. Cancer Cell. 2019 Nov 11;36(5):545–7.

19. Castroviejo-Bermejo M, Cruz C, Llop Guevara A, Gutiérrez Enríquez S, Ducy M, Ibrahim YH, et al. A RAD51 assay feasible in routine tumor samples calls PARP inhibitor response beyond BRCA mutation. EMBO Mol Med. 2018 Dec 7;10(12):e9172–16.

20. Velazquez C, Orhan E, Tabet I, Fenou L, Orsetti B, Adélaïde J, et al. BRCA1-methylated triple negative breast cancers previously exposed to neoadjuvant chemotherapy form RAD51 foci and respond poorly to olaparib. Frontiers in Oncology. 2023;13:1125021.

21. Manoir du S, Orsetti B, Bras-Gonçalves R, Nguyen T-T, Lasorsa L, Boissière F, et al. Breast tumor PDXs are genetically plastic and correspond to a subset of aggressive cancers prone to relapse. Molecular Oncology. 2014 Mar;8(2):431–43.

22. Colombo P-E, Manoir du S, Orsett B, Bras-Gonçalves R, Lambros MB, Mackay A, et al. Ovarian carcinoma patient derived xenografts reproduce their tumor of origin and preserve an oligoclonal structure. Oncotarget. 2015 Sep 29;6(29):28327–40.

23. Tosi D, Pérez-Gracia E, Atis S, Vié N, Combès E, Gabanou M, et al. Rational development of synergistic combinations of chemotherapy and molecular targeted agents for colorectal cancer treatment. BMC Cancer. 2018 Aug 13;18(1):812.

24. Wang Y, Bernhardy AJ, Cruz C, Krais JJ, Nacson J, Nicolas E, et al. The BRCA1- 11q Alternative Splice Isoform Bypasses Germline Mutations and Promotes Therapeutic Resistance to PARP Inhibition and Cisplatin. Cancer Res. 2016 May 1;76(9):2778–90.

25. Abbotts R, Dellomo AJ, Rassool FV. Pharmacologic Induction of BRCAness in BRCA-Proficient Cancers: Expanding PARP Inhibitor Use. Cancers (Basel). 2022 May 26;14(11).

26. Johnson N, Li Y-C, Walton ZE, Cheng KA, Li D, Rodig SJ, et al. Compromised CDK1 activity sensitizes BRCA-proficient cancers to PARP inhibition. Nat Med. 2011 Jul;17(7):875–82.

27. Emadi F, Teo T, Rahaman MH, Wang S. CDK12: a potential therapeutic target in cancer. Drug Discovery Today. 2020 Dec;25(12):2257–67.

28. Ekumi KM, Paculova H, Lenasi T, Pospichalova V, Bösken CA, Rybarikova J, et al. Ovarian carcinoma CDK12 mutations misregulate expression of DNA repair genes via deficient formation and function of the Cdk12/CycK complex. Nucleic Acids Res. 2015 Mar 11;43(5):2575–89.

29. Bajrami I, Frankum JR, Konde A, Miller RE, Rehman FL, Brough R, et al. Genome-wide Profiling of Genetic Synthetic Lethality Identifies CDK12 as a Novel Determinant of PARP1/2 Inhibitor Sensitivity. Cancer Res. 2014 Jan 5;74(1):287–97.

30. Olson CM, Jiang B, Erb MA, Liang Y, Doctor ZM, Zhang Z, et al. Pharmacological perturbation of CDK9 using selective CDK9 inhibition or degradation. Nature Chemical Biology. 2018 Feb;14(2):163–70.

31. Johannes JW, Denz CR, Su N, Wu A, Impastato AC, Mlynarski S, et al. Structure-Based Design of Selective Noncovalent CDK12 Inhibitors. ChemMedChem. 2018 Feb 6;13(3):231–5.

32. Parry D, Guzi T, Shanahan F, Davis N, Prabhavalkar D, Wiswell D, et al. Dinaciclib (SCH 727965), a novel and potent cyclin-dependent kinase inhibitor. Molecular Cancer Therapeutics. 2010 Aug;9(8):2344–53.

33. Rajput S, Khera N, Guo Z, Hoog J, Li S, Ma CX. Inhibition of cyclin dependent kinase 9 by dinaciclib suppresses cyclin B1 expression and tumor growth in triple negative breast cancer. Oncotarget. 2016 Aug 30;7(35):56864–75.

34. Mita MM, Mita AC, Moseley JL, Poon J, Small KA, Jou Y-M, et al. Phase 1 safety, pharmacokinetic and pharmacodynamic study of the cyclin-dependent kinase inhibitor dinaciclib administered every three weeks in patients with advanced malignancies. Br J Cancer. 2017 Oct 24;117(9):1258–68.

35. Carey JPW, Karakas C, Bui T, Chen X, Vijayaraghavan S, Zhao Y, et al. Synthetic Lethality of PARP Inhibitors in Combination with MYC Blockade Is Independent of BRCA Status in Triple-Negative Breast Cancer. Cancer Res. 2018 Feb 1;78(3):742–57.

36. Hossain DMS, Javaid S, Cai M, Zhang C, Sawant A, Hinton M, et al. Dinaciclib induces immunogenic cell death and enhances anti-PD1-mediated tumor suppression. J Clin Invest. 2018 Feb 1;128(2):644–54.

37. Shapiro GI, Do KT, Tolaney SM, Hilton JF, Cleary JM, Wolanski A, et al. Abstract CT047: Phase 1 dose-escalation study of the CDK inhibitor dinaciclib in combination with the PARP inhibitor veliparib in patients with advanced solid tumors. Cancer Res. 2017 Jul 1;77(13_Supplement):CT047–7.

Gene	Forward	Reverse
BRCA1	TCCAAACCTGTGTCAAGCTG	CTTATTCCATTCTTTTCTCTCACACAG
BRCA1	GATTCTGCAAAAAAGGCTGCT	CAGATGCTGCTTCACCCTGA
BRCA2	TACAGTTGGCTGATGGTGGA	CCATAGCTGCCAGTTTCCAT
53BP1	TGGTTCCATCAGTCAGGTCA	CCTCAGCACCAAGGGAATGT
RAD51	CAGTGATGTCCTGGATAATGTAGC	TTACCACTGCTACACCAAACTCAT
PALB2	CCCAGCATCAGATCATTGTG	ATGAAATGGAGCCGTGAAAG
CHEK1	GCTCCTCTAGCTCTGCTGCATAAA	ACTCTGACACACCACCTGAAGTGA
ATM	CTGCAGAGAAACACGGAAAC	CCTGTGCACCATTCAAGAAC
ATR	CCAGGCATCCTCCTATTTTTC	TTTTCACCATGACGGTCTCC
PARP1	GAGTCGAGTACGCCAAGAGC	TCAGAGAACCCATCCACCTC
GAPDH	TGCACCACCACCTGCTTAGC	GGCATGGACTGTGGTCATGAG

Table 1: list of primers used in Q-RTPCR experiments. Sequences are presented 3' to 5'

PDX ID	Cancer type	Grade /Stage	BRCA1 Status	BRCA1 protein expression	BRCA2 status	Olaparib response	53BP1 Protein	PARP1 Protein
b3804	TNBC	SBR III	WT	Full length and δ11 variant	WT/normal expression	Non responsive	detectable	normal
b1995	TNBC	SBR III	WT	Full length	WT/normal expression	Non responsive	detectable	normal
b3977	TNBC	SBR III	Me/Me	Not detectable	WT/normal expression	Non responsive	Not detectable	reduced
15b0018	TNBC	SBR II	Me/Me	Not detectable	WT/normal expression	Non responsive	detectable	reduced
b4122	TNBC	SBR III	Me/Me	Not detectable	WT/normal expression	Responsive	Not detectable	normal
o10047	HGOC	Stage IV	Mut Del exon 8-13	Not detectable	WT no protein expression	Responsive	detectable	normal

Table 2: principal characteristics of the PDX models used in this study. HGOC: High Grade Ovarian Carcinoma. SBRIII: Scarff, Bloom and Richardson tumor grade III. WT: Wild type sequence. Me/Me homozygous hypermethylation of the promoter. Non-responsive indicates a tumor that progressed under olaparib treatment. Responsive: stabilized or reduced tumor size under treatment.

Figure legends

Figure 1: dinaciclib and SR-4835 increase the sensitivity of TNBC cells to olaparib. A: TNBC cell lines show differential drug sensitivity according to their BRCA1 status; IC50 box plots stratified according BRCA1-WT (BRCA-proficient), BRCA1-Def (BRCA-deficient), BRCA1-Def-RE (olaparib resistant). **B:** dinaciclib is synergistic in combination with olaparib as shown by synergy matrices of dinaciclib and olaparib combination treatment in BT-549, SUM159 and MDA-MB-436 cell lines. Numbers on the X and Y indicate nanomolar drug concentrations. Synergy is indicated by red boxes corresponding to above than expected levels of toxicity. Green boxes indicate antagonism and black boxes correspond to additive effect. Blue arrow-heads indicate the range of synergistic dinaciclib concentrations. **C:** synergy matrices of SR-4835 in combination with olaparib. Experimental setting was identical to that used with dinaciclib. **D:** dinaciclib and SR-4835 introduced at 1nM or 10nM reduce the concentrations of olaparib needed to reach IC50 in TNBC BCCLs by a factor 10 to 1000 (see also Supplementary Figure 1B). IC50 concentrations were normalized to those measured with olaparib in mono and concentration reduction levels were determined calculating the ratio IC50combo/IC50mono. **E, F:** cell mortality assessed by FACS quantification of the annexin and/or PI positive cell fractions in SUM159B1 and SUM159B1KO. Statistical significance was determined using the Student t test; * indicates p=0.05, ** p=0.01, *** p=0.001.

Figure 2: respective impact of dinaciclib and SR-4835 on HR gene expression and nuclear foci formation in the BRCA1-WT SUM159 BCCL. A: level of mRNA expression changes resulting from combos with dinaciclib (dina) or SR-4835 (SR). mRNA gene expression levels were determined by Q-RTPCR and presented as fold change differences in treated vs. control (DMSO) conditions. **B:** impact of dinaciclib and SR-4835 on protein expression of the principal actors of the HR pathway in SUM-159 BRCA1-WT cells. **C, D, E:** dinaciclib and SR-4835 reduce olaparib induced BRCA1 and RAD51 nuclear foci formation, examples of immunofluorescence fields (C), quantification of BRCA1 nuclear foci (D), quantification of RAD51 nuclear foci (E). **F, G:** siRNA attenuation of CDK9 or CDK12 or CDK13 RNA expression has differential impact on RAD51 and BRCA1 nuclear foci formation, examples of immunofluorescence fields (F), quantification of BRCA1 (green bars) and RAD51 (ref bars) nuclear foci (G). Nuclear foci were quantified on a minimum of 200 cell nuclei per microscopic field.

Figure 3: Dinaciclib and SR-4835 treatment reduce BRCA1 and RAD51 nuclear foci formation in olaparib-resistant BRCA1-deficient cell models. A: immunofluorescence detection of BRCA1 and RAD51 nuclear foci in BRCA1KO SUM159B1KO and its olaparib resistant variant SUM159B1KO-Re. **B, C:** BRCA1 and RAD51 nuclear foci quantification in SUM159B1KO and SUM159B1KO-Re. D: immunofluorescence detection of BRCA1 and RAD51 nuclear foci in SUM149PT (BRCA1 deficient) and SUM149-RE (olaparib resistant variant). **E, F:** BRCA1 and RAD51 foci quantification in SUM149PT and SUM149-RE. **G:** immunofluorescence detection of BRCA1 and RAD51 nuclear foci in UWB1.289PT (BRCA1 deficient) and UWB1.289RE (olaparib resistant variant). **H, I:** quantification of BRCA1 and RAD51 foci in UWB1.289PT and UWB1.289RE. BRCA1 and RAD51 nuclear foci were scored as in Figure 2.

Figure 4: dinaciclib increases olaparib sensitivity of PDX models. A: tumor volume changes of individual PDX grafts observed in the 3 treatment arms (vehicle (grey), olaparib (blue), olaparib + dinaciclib(red)). Tumor volume changes normalized on starting PDX graft volumes were computed at the end of treatment. **B:** BRCA1 and RAD51 Immunofluorescence staining in sections from PDX tumors sampled at treatment end. **C, D :** Quantification of BRCA1 and RAD51 foci in the respective PDX models. Nuclear foci numbers were scored as in Figure 2. Statistical significance was determined using the Student t test; * indicates p=0.05, ** p=0.01, *** p=0.001.

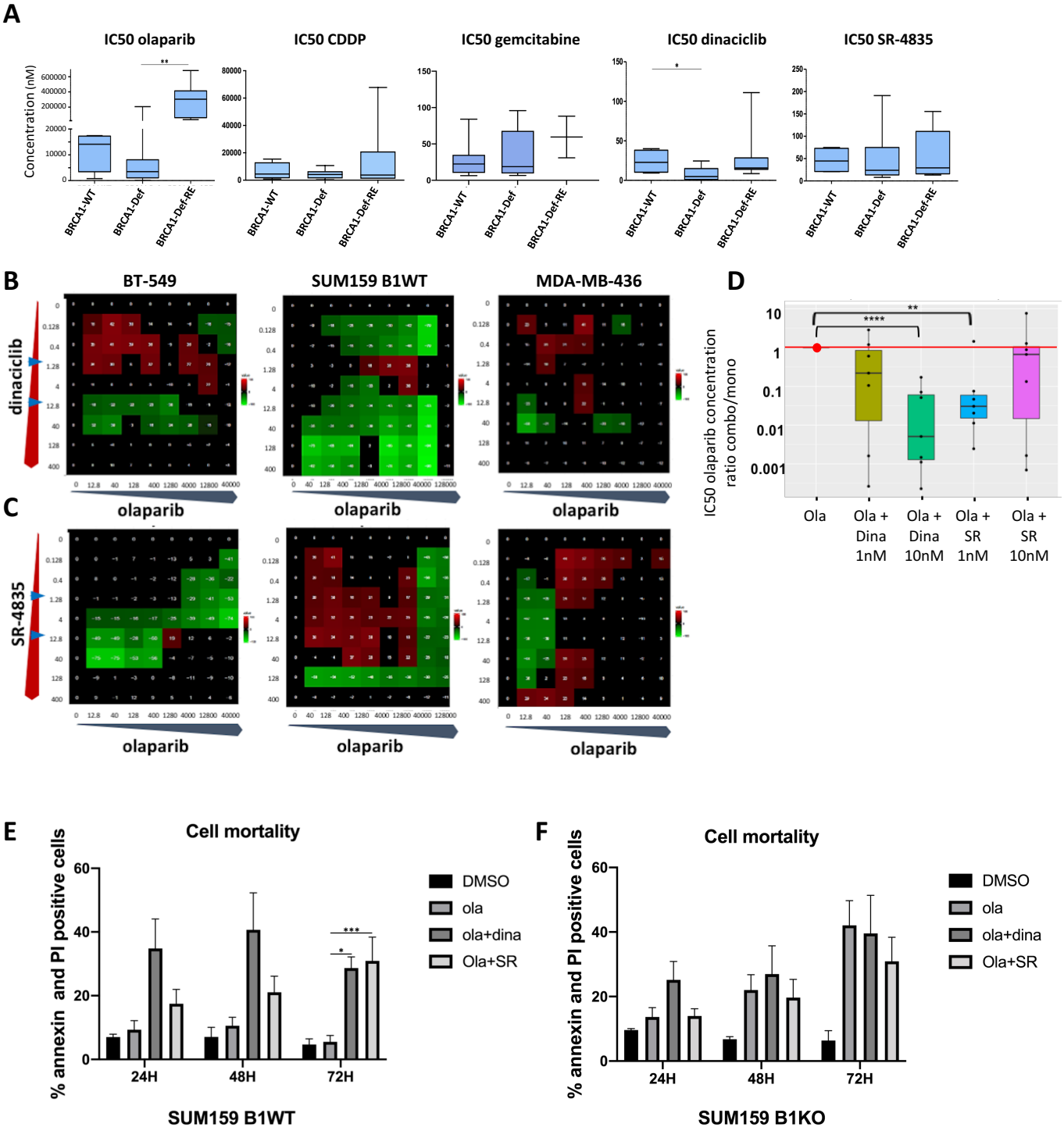
A
IC50 olaparib
IC50 CDDP
IC50 gemcitabine
IC50 dinaciclib
IC50 SR-4835
Concentration (nM)
BRCA1-WT
BRCA1-Def
BRCA1-Def-RE
B
BT-549
SUM159 B1WT
MDA-MB-436
dinaciclib
olaparib
C
SR-4835
olaparib
D
IC50 olaparib concentration ratio combo/mono
Ola
Ola + Dina 1nM
Ola + Dina 10nM
Ola + SR 1nM
Ola + SR 10nM
E
Cell mortality
% annexin and PI positive cells
DMSO
ola
ola+dina
Ola+SR
24H
48H
72H
SUM159 B1WT
F
Cell mortality
% annexin and PI positive cells
DMSO
ola
ola+dina
Ola+SR
24H
48H
72H
SUM159 B1KO

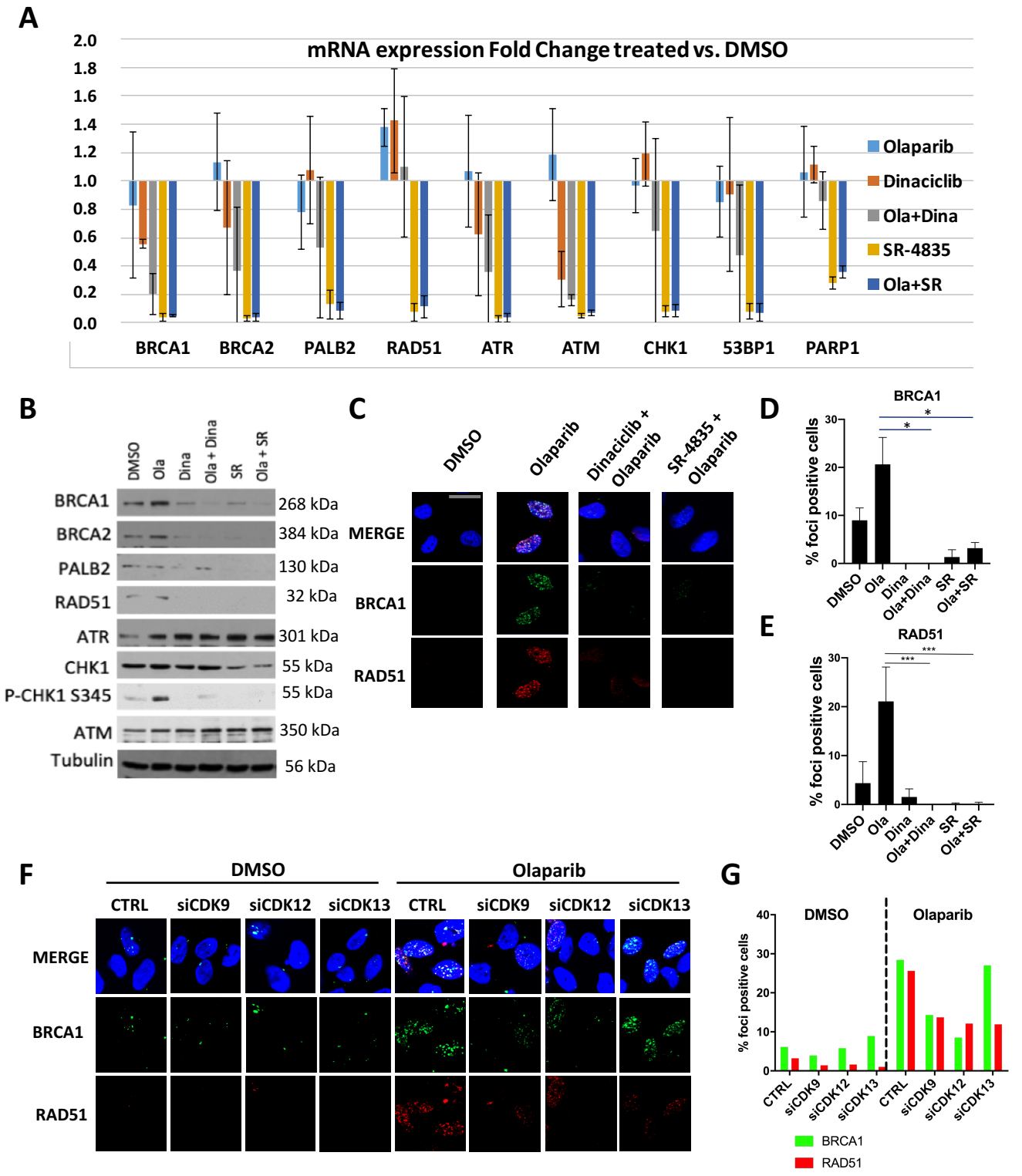

Figure 2: respective impact of dinaciclib and SR-4835 on HR gene expression and nuclear foci formation in the BRCA1-WT SUM159 BCCL. **A:** level of mRNA expression changes resulting from combos with dinaciclib (dina) or SR-4835 (SR). mRNA gene expression levels were determined by Q-RTPCR and presented as fold change differences in treated vs. control (DMSO) conditions. **B:** impact of dinaciclib and SR-4835 on protein expression of the principal actors of the HR pathway in SUM-159 BRCA1-WT cells. **C, D, E:** dinaciclib and SR-4835 reduce olaparib induced BRCA1 and RAD51 nuclear foci formation, examples of immunofluorescence fields (C), quantification of BRCA1 nuclear foci (D), quantification of RAD51 nuclear foci (E). **F, G:** siRNA attenuation of CDK9 or CDK12 or CDK13 RNA expression has differential impact on RAD51 and BRCA1 nuclear foci formation, examples of immunofluorescence fields (F), quantification of BRCA1 (green bars) and RAD51 (ref bars) nuclear foci (G). Nuclear foci were quantified on a minimum of 200 cell nuclei per microscopic field.

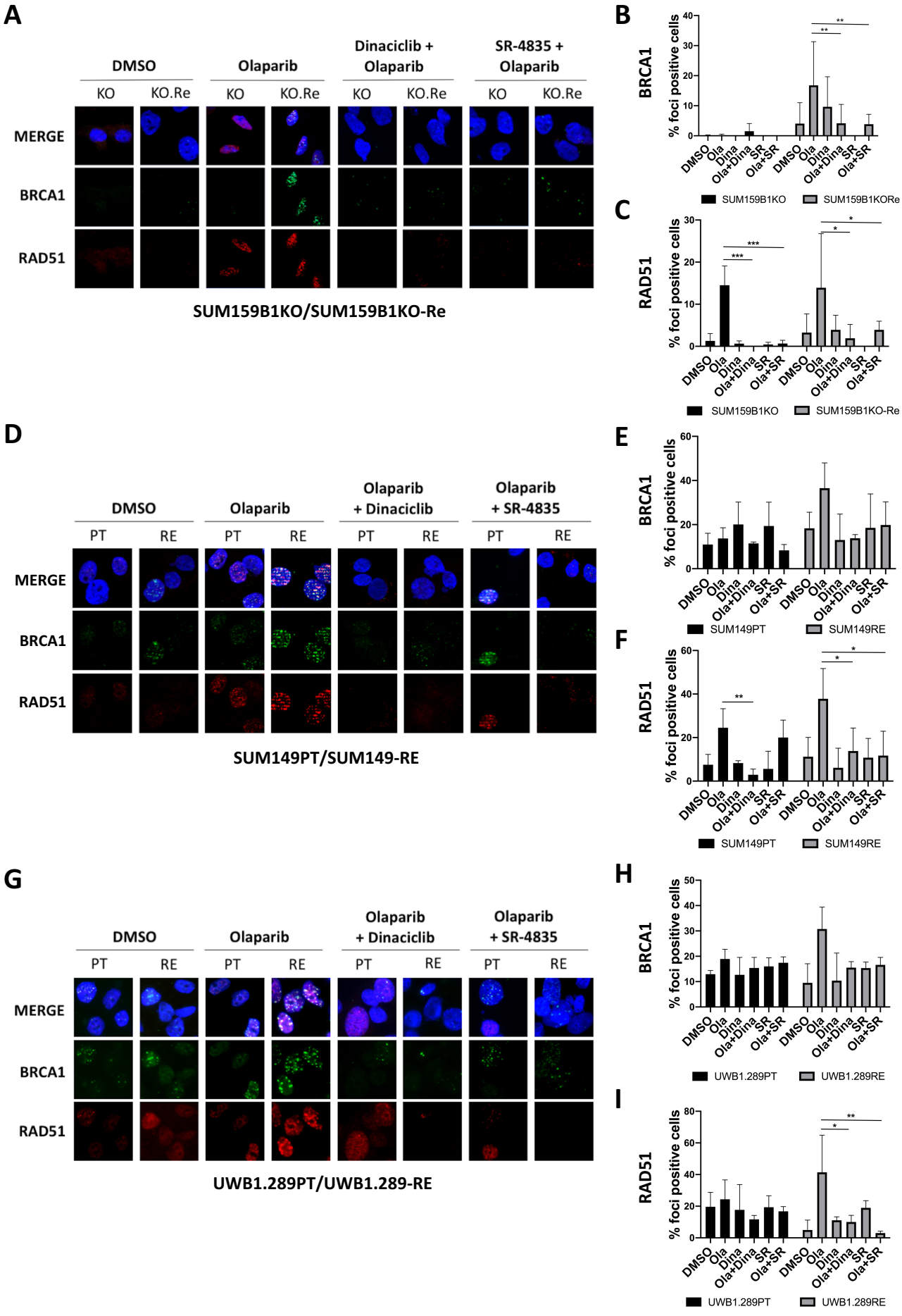
A
DMSO
Olaparib
Dinaciclib + Olaparib
SR-4835 + Olaparib
KO
KO.Re
MERGE
BRCA1
RAD51
SUM159B1KO/SUM159B1KO-Re
B
BRCA1
% foci positive cells
SUM159B1KO
SUM159B1KORe
C
RAD51
% foci positive cells
SUM159B1KO
SUM159B1KO-Re
D
DMSO
Olaparib
Olaparib + Dinaciclib
Olaparib + SR-4835
PT
RE
MERGE
BRCA1
RAD51
SUM149PT/SUM149-RE
E
BRCA1
% foci positive cells
SUM149PT
SUM149RE
F
RAD51
% foci positive cells
SUM149PT
SUM149RE
G
DMSO
Olaparib
Olaparib + Dinaciclib
Olaparib + SR-4835
PT
RE
MERGE
BRCA1
RAD51
UWB1.289PT/UWB1.289-RE
H
BRCA1
% foci positive cells
UWB1.289PT
UWB1.289RE
I
RAD51
% foci positive cells
UWB1.289PT
UWB1.289RE
DMSO
Ola
Dina
Ola+Dina
SR
Ola+SR

Figure 3: **Dinaciclib and SR-4835 treatment reduce BRCA1 and RAD51 nuclear foci formation in olaparib-resistant BRCA1-deficient cell models. A:** immunofluorescence detection of BRCA1 and RAD51 nuclear foci in BRCA1KO SUM159B1KO and its olaparib resistant variant SUM159B1KO-Re. **B, C**: BRCA1 and RAD51 nuclear foci quantification in SUM159B1KO and SUM159B1KO-Re. **D:** immunofluorescence detection of BRCA1 and RAD51 nuclear foci in SUM149PT (BRCA1 deficient) and SUM149-RE (olaparib resistant variant). **E, F**: BRCA1 and RAD51 foci quantification in SUM149PT and SUM149-RE. **G:** immunofluorescence detection of BRCA1 and RAD51 nuclear foci in UWB1.289PT (BRCA1 deficient) and UWB1.289RE (olaparib resistant variant). **H, I:** quantification of BRCA1 and RAD51 foci in UWB1.289PT and UWB1.289RE. BRCA1 and RAD51 nuclear foci were scored as in Figure 2.

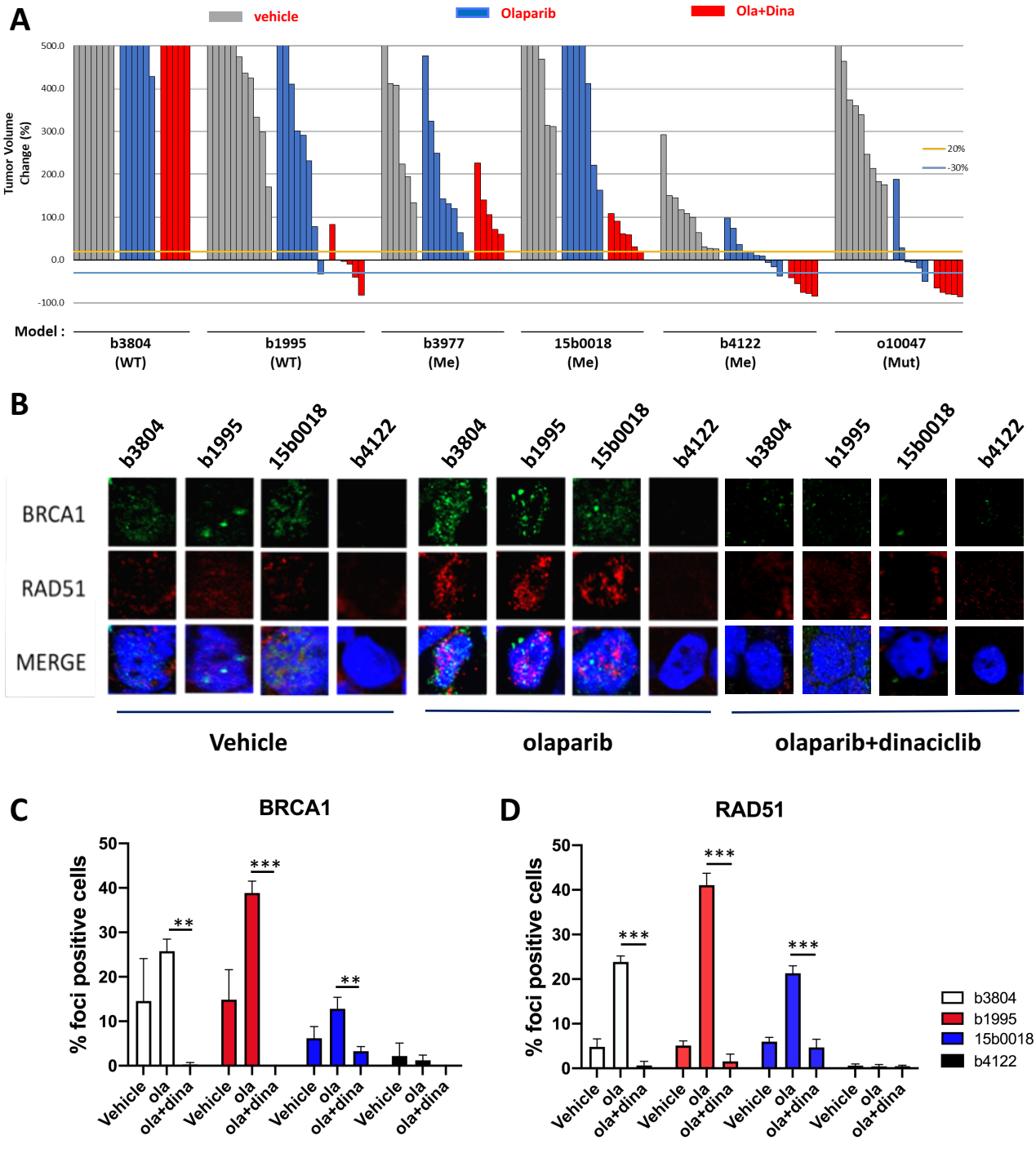

Figure 4: dinaciclib increases olaparib sensitivity of PDX models. A: tumor volume changes of individual PDX grafts observed in the 3 treatment arms (vehicle (grey), olaparib (blue), olaparib + dinaciclib(red)). Tumor volume changes normalized on starting PDX graft volumes were computed at the end of treatment. **B:** BRCA1 and RAD51 Immunofluorescence staining in sections from PDX tumors sampled at treatment end. **C, D :** Quantification of BRCA1 and RAD51 foci in the respective PDX models. Nuclear foci numbers were scored as in Figure 2. Statistical significance was determined using the Student t test ; * indicates p=0.05, ** p=0.01, *** p=0.001.

Figure 1: dinaciclib and SR-4835 increase the sensitivity of TNBC cells to olaparib. A: TNBC cell lines show differential drug sensitivity according to their BRCA1 status; IC50 box plots stratified according BRCA1-WT (BRCA-proficient), BRCA1-Def (BRCA-deficient), BRCA1-Def-RE (olaparib resistant). **B:** dinaciclib is synergistic in combination with olaparib as shown by synergy matrices of dinaciclib and olaparib combination treatment in BT-549, SUM159 and MDA-MB-436 cell lines. Numbers on the X and Y indicate nanomolar drug concentrations. Synergy is indicated by red boxes corresponding to above than expected levels of toxicity. Green boxes indicate antagonism and black boxes correspond to additive effect. Blue arrow-heads indicate the range of synergistic dinaciclib concentrations. **C:** synergy matrices of SR-4835 in combination with olaparib. Experimental setting was identical to that used with dinaciclib. **D:** dinaciclib and SR-4835 introduced at 1nM or 10nM reduce the concentrations of olaparib needed to reach IC50 in TNBC BCCLs by a factor 10 to 1000 (see also Supplementary Figure 1C). IC50 concentrations were normalized to those measured with olaparib in mono and concentration reduction levels were determined calculating the ratio IC50combo/IC50mono (see Supplementary Figure 1B for IC50 changes in indvidual cell lines). **E, F:** cell mortality assessed by FACS quantification of the annexin and/or PI positive cell fractions in SUM159B1 and SUM159B1KO.

A

	BRCA-status	Cell line / Drug	Olaparib	CDDP	Gemcitabine	Dinaciclib (CDKi)	SR-4835 (CDK12/13i)	Mutations in other DDR genes
BRCA1-proficient	BRCAwt	BT-549	16741	15427	22.46	40.13	20.66	***FANCL, POLQ***
	BRCAwt	HCC-1143	777.4	919.6	10.23	9.327	22.21	***ERCC6***
	BRCAwt	SUM159 B1.22 (WT)	17457	6221	6.496	13.25	74.89	
	BRCAwt	SUM159 WT	11481	2833	33.08	32.34	66.96	
	Ectopic BRCA1	UWB1 + B1	315610	29635	12.13	2.272	36.2	
BRCA1-deficient	CRISPR BRCA1-null	SUM159 B1.22.2 (KO)	2928	1328	7.53	0.9434	63.04	
	CRISPR RAD51C-null	SUM159.RAD51C-KO	764.8	1265	66.36	11.34	21.18	
	CRISPR RAD51D-null	SUM159.RAD51D-KO	77.9	291.4	14.1	24.6	18.39	
	BRCA1-null	MDA-MB-436	4928	10730	15.21	16.13	78.77	***FANCI***
	BRCA1 methylated	HCC-38	2015	5247	56.43	1.304	8.067	***TOP1, 53BP1***
	BRCA1 methylated	OVCAR8	9141	3059	6.683	0.6877	26.4	***ATM, CDC25A, REV3L***
	BRCA1-Delta 11	SUM149 PT	205438	6964	19.45	3.542	11.83	***FANCD2***
	BRCA1-Delta 11	UWB1 PT	4008	5448	95.8	6.204	191.1	***BRIP1, MSH2***
BRCA1-deficent Olaparib resistant	BRCA-def ola.resistant	SUM159 B1.22.2 KO-Re	60415	1025	173.4	13.9	15.97	
	BRCA-def ola.resistant	HCC-38 Re	34281	1552	24.81	8.55	27.95	
	BRCA-def ola.resistant	OVCAR8 Re	303104	3746	15.97	28.38	110.9	
	BRCA-def ola.resistant	SUM149 Re	682569	11806	88.01	111.1	13.33	
	BRCA-def ola.resistant	UWB1 R BULK	330692	67770	30.77	15.74	155.6	

B

BRCA-status	Cell line / Drug	Olaparib	Ola/Dina 1nM	ratio mono/combo	Ola/Dina 10nM	ratio mono/combo	Ola/SR 1nM	ratio mono/combo	Ola/SR 10nM	ratio mono/combo
BRCAwt	BT-549	16741	12998	1.3	7990	2.1			1197	14.0
BRCAwt	HCC-1143	777.4	9341	0.1	4195	0.2	10115	0.08	3154	0.2
BRCAwt	SUM159B1	17457	4.7	3724.6	4.03	4317.8	535	32.62	15315	1.1
BRCAwt	SUM159	11481	921	12.5	59810	0.2	70165	0.16	892.5	13.0
Ectopic BRCA1	UWB1 + B1	315610	67821	4.7	45746	6.9	12348	25.56	1424	221.6
CRISPR BRCA1-null	SUM159 B1.22.2 (KO)	2928	4.85	603.0	4.4	663.2	33.7	87.0	3812	0.8
CRISPR RAD51C-null	SUM159.RAD51C-KO	765.0	5525	0.1	1288	0.6	40.03	19.11	32.0	24.0
CRISPR RAD51D-null	SUM159.RAD51D-KO	78.0	25.34	3.1	7723	0.00	1360	0.06	10.55	7.4
BRCA1-null	MDA-MB-436	4928	5325	0.9	5916	0.8	207.0	24.0	417	12.00
BRCA1 methylated	HCC-38	2015	7725	0.3	22.07	91.3	8231	0.24	302.0	6.7
BRCA1-Delta 11	SUM149 PT	205438	45074	4.6	1046	196.4	4185	49.1	355	578.7
BRCA1-Delta 11	UWB1 PT	4008	4767	0.8	284	14.1	186	21.55	30565	0.1
BRCA-def ola.resistant	SUM159B1KO-Re	60415	172000	0.4	600	100.7	51600	1.2	17800	3.4
BRCA-def ola.resistant	SUM149-ola-Re	682569	71847	9.5	756.2	902.6	51200	13.33	472	1446.1
BRCA-def ola.resistant	UWB1.289-ola-Re	330692	19688	16.8	1679	197.0	81	4082.6	4357	76.0

Supplementary Fig 1: relative levels of sensitivity to olaparib, CDDP, gemcitabine, dinaciclib and SR-4835 in our panel of BRCA1 proficient, BRCA1 deficient and BRCA1 deficient - olaparib resistant cell line models. **A**: mean drug concentrations (nM) used to reach IC50 in individual cell lines. **B:** combinations of dinaciclib and SR-4835 reduce the olaparib concentrations needed to reach IC50 (compare olaparib, ola + dina values and ola + SR). Dinaciclib and SR-4835 were introduced at 2 fixed concentrations; 1 and 10 nM. The levels of olaparib IC50 reduction obtained with dinaciclib or SR-4835 co-treatment are indicated in the IC50-combo/IC50-mono column. Cell viability curves used to determine IC50 levels in panel A and panel B are presented in annexe at the end of the Supplementary Figures. IC50 determination resulted from 12 replicated experiments (3 biological replicates and 4 technical replicates).

A

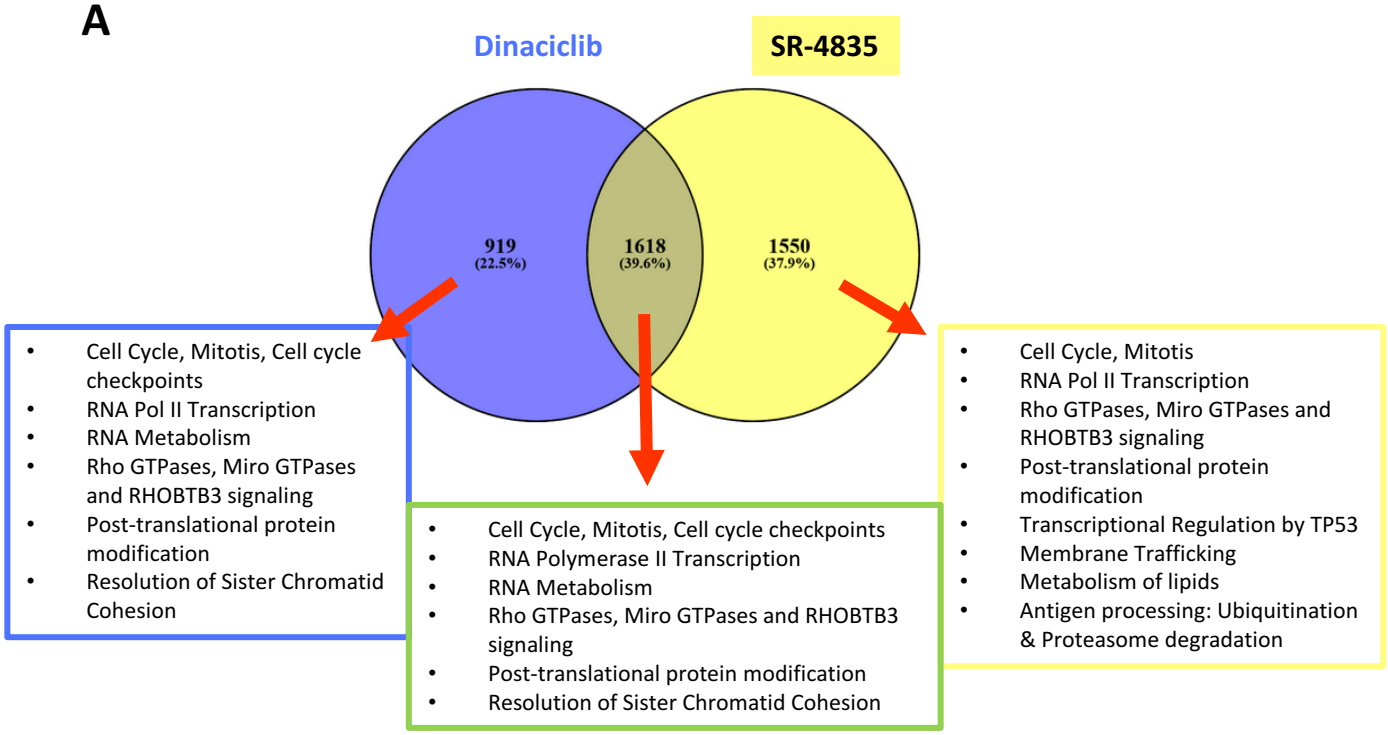

B

Most significantly downregulated pathways by dinaciclib and SR-4835

Dinaciclib vs. DMSO

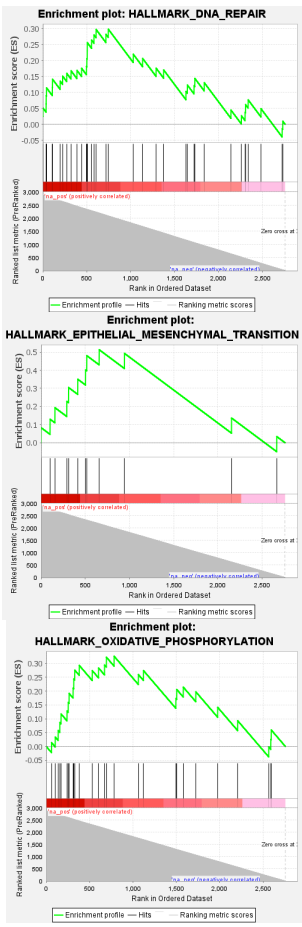

SR-4835 vs. DMSO

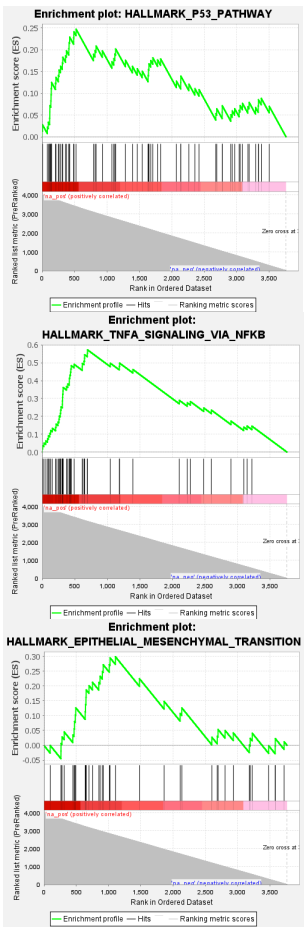

Supplementary Figure 2: dinaciclib and SR-4835 downregulate common pathways but can affect different genes. **A**: number of genes respectively downregulated in SUM159B1 treated with dinaciclib and SR-4835 and impinged corresponding pathways. **B**: selection of most significantly downreglulated pathways by dinaciclib and SR-4835.

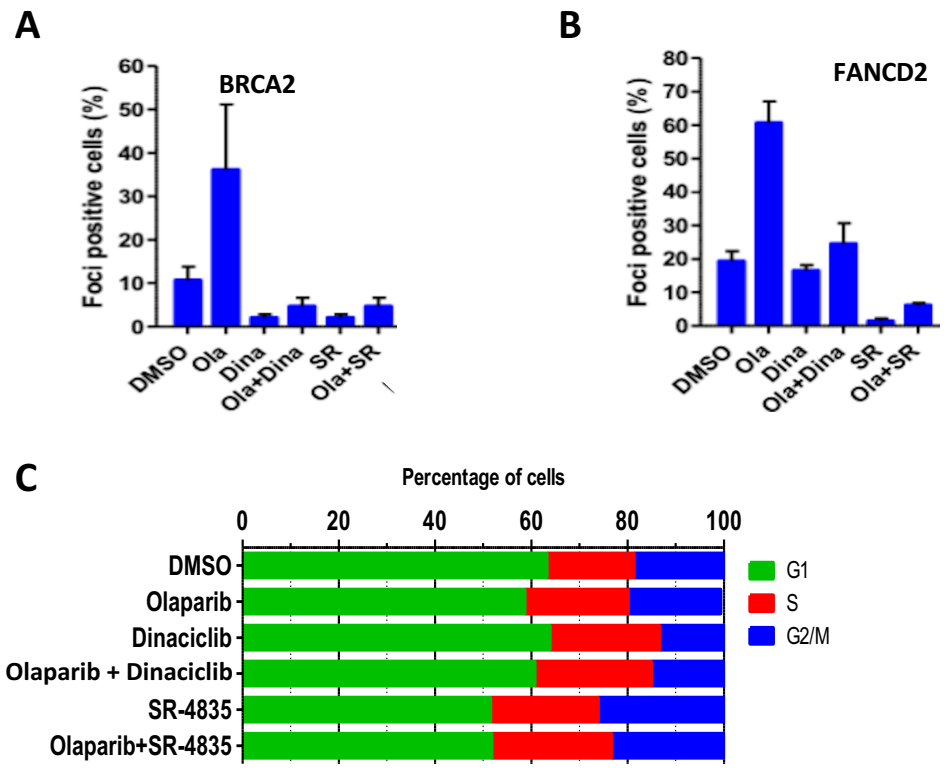

Supplementary Fig 3: A, B : Dinaciclib and SR-4835 addition results in the reduction of BRCA2 and FANCD2 nuclear foci numbers in olaparib-treated SUM159 cells. Nuclear foci were scored as in Figure 2 **C**: cell cycle profiles of dinaciclib and SR-4835 treated SUM159 cells determined by FACS analysis do not show major changes in comparison with olaparib treated cells.

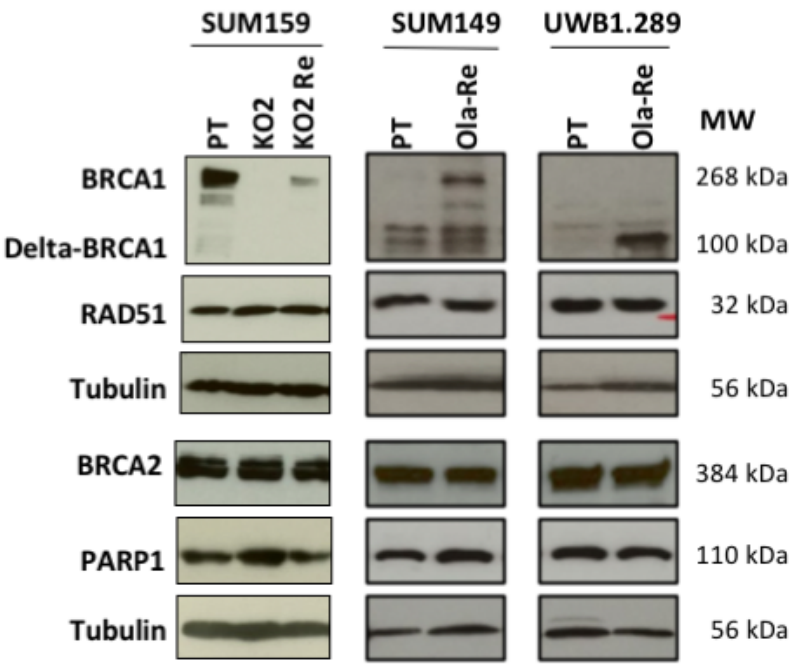

Supplementary Figure 4: Protein expression profiles of the principal HR actors in SUM159B1KO, SUM159B1KO-Re, SUM149PT and SUM149-Ola-Re, UWB1.289PT and UWB1.289-Ola-Re

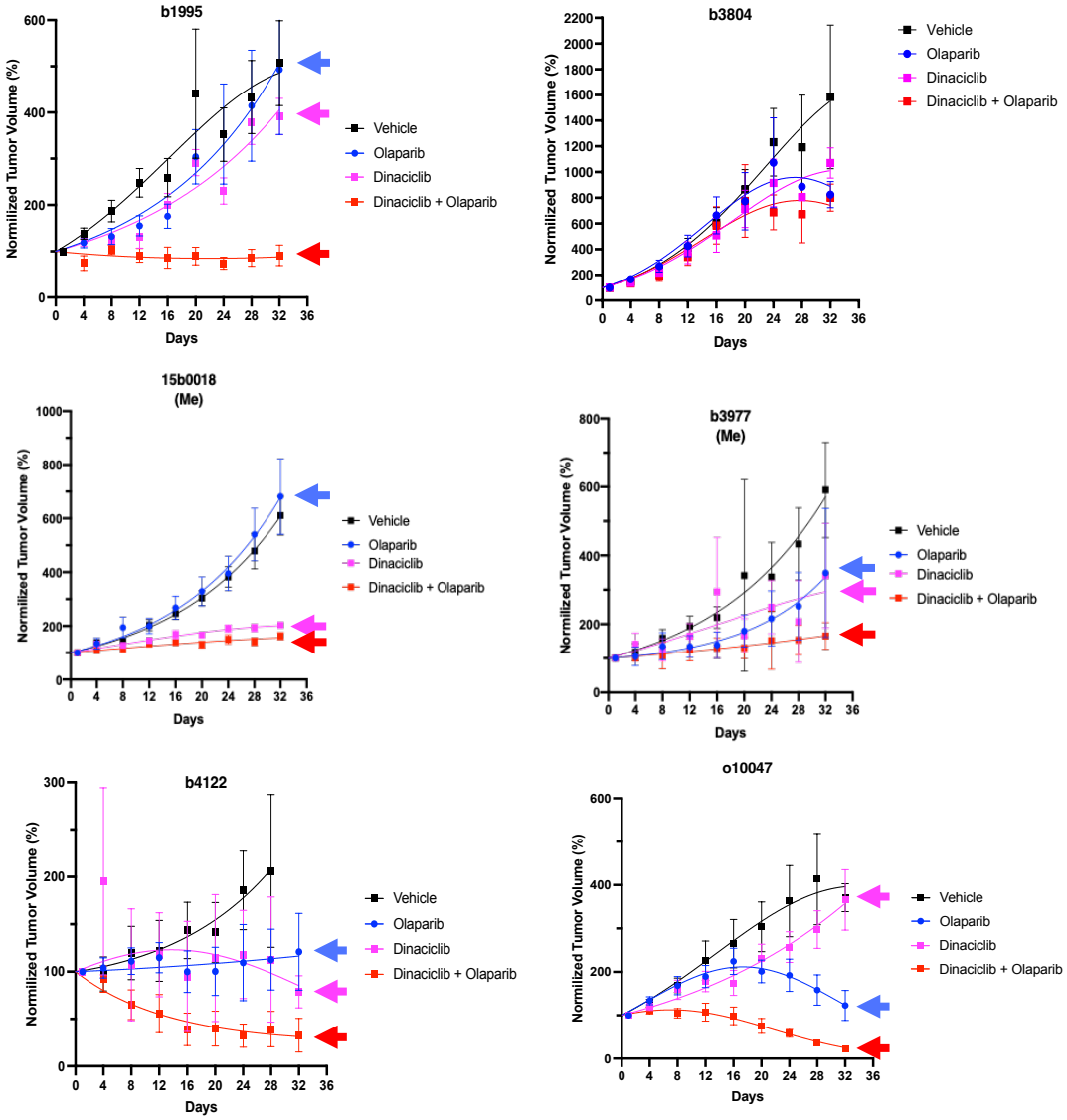

Supplementary Fig 5: mean tumor volume changes of the 6 PDX models tested for the response to olaparib-mono and olaparib+dinaciclib combination. Mean tumor volume (TV) curves are presented for each experimental arm (vehicle, Olaparib, dinaciclib, olaparib+dinaciclib). These curves correspond to PDX tumor volume changes presented in Figure 4A. Olaparib was administrated by oral gavage at 100mg/kg 5days/week for 5weeks. Dinaciclib was injected intraperitoneally at 30mg/kg twice every week for 5weeks.

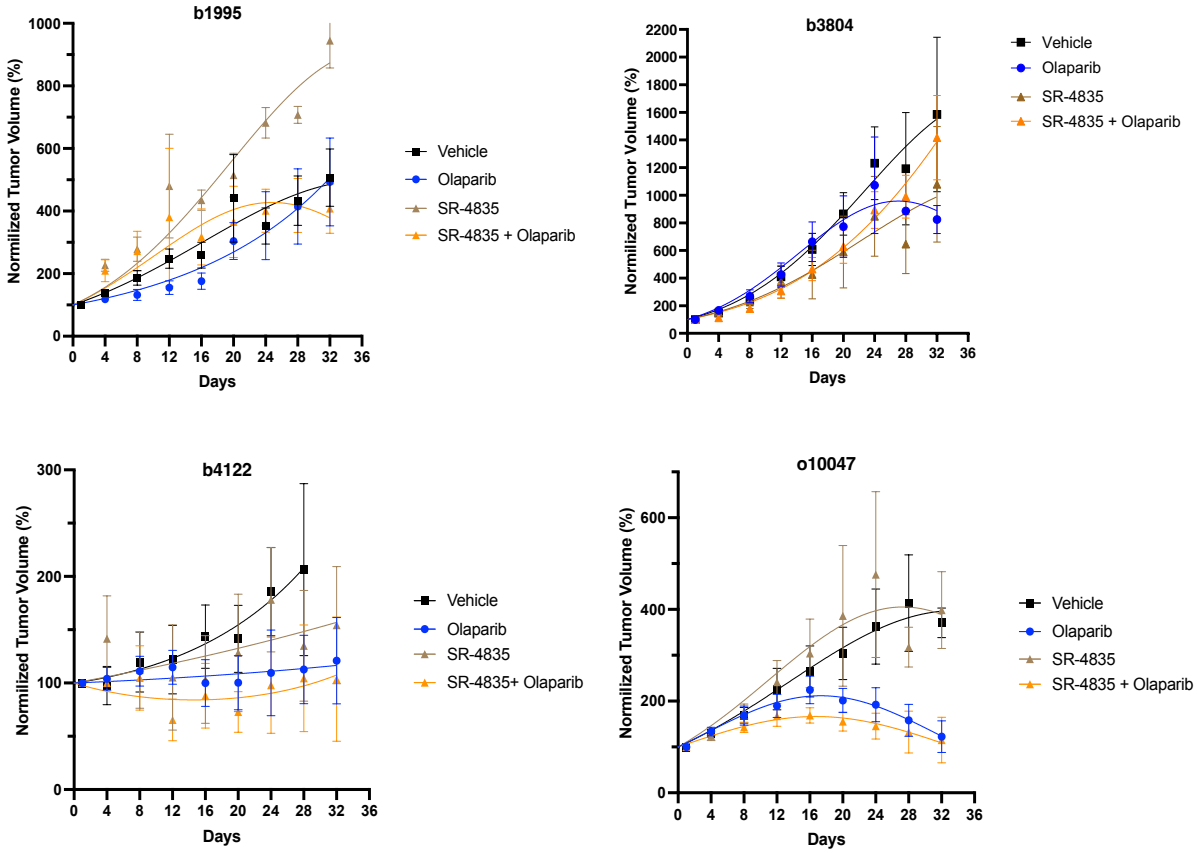

Supplementary Fig 6: mean tumor volume changes of the 6 PDX models tested for the response to olaparib-mono and olaparib+dinaciclib combination. Mean tumor volume (TV) curves are presented for each experimental arm (vehicle, Olaparib, SR-4835, olaparib+SR-4835). Olaparib was administrated by oral gavage at 100 mg/kg 5days/week for 5 weeks. SR-4835 was administrated orally at 30mg/kg twice every week for 5 weeks.

A

Drug / cell line	CDDP	CDDP/Dina 1nM	Ratio mono/ combo	CDDP/Dina 10nM	Ratio mono/ combo	CDDP/SR 1nM	Ratio mono/ combo	CDDP/SR 10nM	Ratio mono/ combo
BT-549	15427	1559	9.9	640.5	24.1	576.2	26.8	40.0	387.8
SUM159 B1.22 (WT)	6221	6.8	917.6	4.0	1530.4	9151.0	0.7	164.6	37.8
SUM159 WT	2833	5037	0.6	4632	0.6	1360.0	2.1	1195.0	2.4
SUM159 PURO (51Cwt)	8980	7566	1.2	5778	1.6	7608.0	1.2	5420.0	1.7
SUM159 BLAST (51Dwt)	2200	4720	0.5	674.5	3.3	8963.0	0.2	3603.0	0.6
SUM159 mean	5058.5	4332.4	1.2	2772.0	1.8	6770.0	0.7	2595.7	1.9
UWB1 + B1	29635								
SUM159 B1.22.2 (KO)	1328	10.4	127.7	4.4	300.0	1521.0	0.9	5705.0	0.2
SUM159.RAD51C-KO	1265	4165	0.3	3004	0.4	4468.0	0.3	5562.0	0.2
SUM159.RAD51D-KO	291.4	908	0.3	490.5	0.6	728.0	0.4	437.0	0.7
MDA-MB-436	10730	60.2	178.3	5.7	1881.1	2387.0	4.5	1291.0	8.3
HCC-38	5247								
OVCAR8	3059								
SUM149 PT	6964	3287	2.1	633.4	11.0	895.0	7.8	98.7	70.5
UWB1 PT	5448	423.2	13.0	98.4	55.4	49.0	111.3	43.0	127.0
SUM159B122.2.OlaRe									
HCC-38-Re									
SUM149 Re	11806	2003	6.0	304.7	38.7	253.7	46.5	160.3	73.6
UWB1 R BULK	67770	4178	16.2	2608	26.0	85.2	795.6	87.0	781.2

B

Drug IC50 / Cell line	Gemcitabine	Gem/Dina 1nM	mono/ combo	Gem/Dina 10nM	mono/ combo	Gem/SR 1nM	mono/ combo	Gem/SR 10nM	mono/ combo
BT-549	22.46	14.3	1.6	8.73	2.6	7.25	3.1	3.72	6.0
SUM159 B1.22 (WT)	6.5	0.2	31.7	0.42	15.3	0.9	7.3	7.4	0.9
SUM159 WT	33.1	41.0	0.8	4.34	7.6	34.5	1.0	28.0	1.2
SUM159 PURO (51Cwt)	84	24	3.5	11	7.7	27	3.1	11.5	7.3
SUM159 BLAST (51Dwt)	35	0.75	45.3	1.2	28.3	7.3	4.8	7.1	4.9
UWB1 + B1	12.13								
SUM159 B1.22.2 (KO)	7.5	0.34	21.8	0.22	33.4	10.9	0.7	21.1	0.4
SUM159.RAD51C-KO	72	32	2.3	23	3.1	55	1.3	15.0	4.8
SUM159.RAD51D-KO	18.2	8.2	2.2	11	1.7	1.4	13.0	6.5	2.8
MDA-MB-436	15.2	1.8	8.6	5.2	2.9	1.8	8.6	0.44	34.6
HCC-38	56.4								
OVCAR8	6.7								
SUM149 PT	19.45	14.4	1.3	0.65	29.6	1.7	11.3	0.2	96.0
UWB1 PT	95.8	10.0	9.6	0.40	237.0	0.43	221.3	0.6	162.1
SUM159B122.2.OlaRe									
SUM149 Re	88.0	2.25	39.2	0.5	173.7	0.28	315.1	0.1	824.8
UWB1 R BULK	30.77	4.3	7.2	2.4	12.8	0.41	73.9	0.8	38.3

C

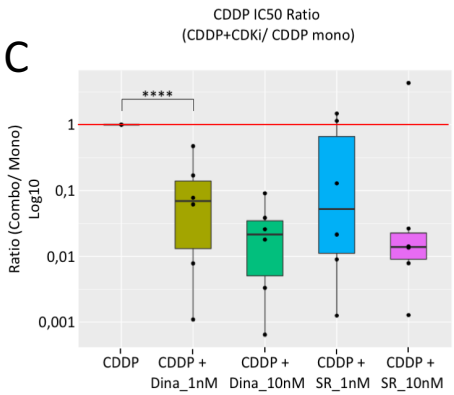

D

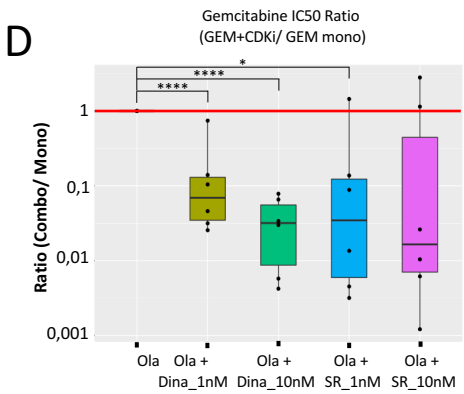

Supplementary Figure 7: **CDKi administered in combination enhance the efficacy of CDDP and gemcitabine by a factor 10 to 100. A:** dinaciclib and SR-4835 introduced at fixed concentrations of 1nM or 10nM reduce the concentrations of CDDP needed to reach IC50 in TNBC BCCLs by a factor 10 to 100 as indicated in the column IC50 combo/IC50 mono. **B:** same as A but with gemcitabine. **C, D**: box plot representation of IC50 changes induced by combination treatments. Concentrations were normalized to their levels measured with CDDP or gemcitabine mono and concentration reduction levels were determined calculating the ratio combo/mono.

Annexe:

Cell viability curves for the IC50 determination in breast and ovarian cancer cell lines

Single drug administration :

Olaparib, Cis-platin (CDDP), Gemcitabine, Dinaciclib, SR-4835

Combinations :

Olaparib + Dinaciclib, Olaparib+ SR-4835, CDDP+ Dinaciclib, CDDP+ SR-4835, Gemcitabine + Dinaciclib, Gemcitabine + SR-4835

Olaparib mono

Courbes de régression non linéaires de la viabilité cellulaire en réponse à l'olaparib

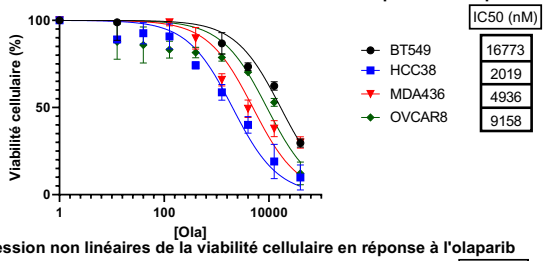

	IC50 (nM)
BT549	16773
HCC38	2019
MDA436	4936
OVCAR8	9158

Courbes de régression non linéaires de la viabilité cellulaire en réponse à l'olaparib (PARPi)

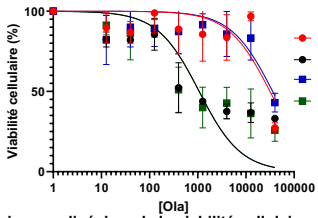

	IC50 (nM)
SUM159 Cas9 Puro	31515
SUM159 Rad51 C	1067
SUM159 Cas9 Blast	35935
SUM159 Rad51 D	1073

Courbes de régression non linéaires de la viabilité cellulaire en réponse à l'olaparib

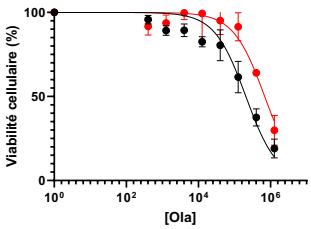

	IC50 (nM)
SUMP149PT	205839
SUM149 Re	684108

Courbes de régression non linéaires de la viabilité cellulaire en réponse à l'olaparib (PARPi)

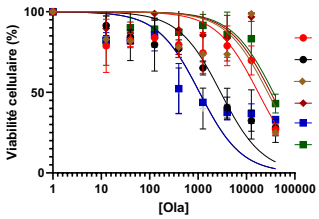

	IC50 (nM)
SUM159 B1.22	17489
SUM159 B1.22.2	2928
SUM159 Cas9 Puro	27489
SUM159 Rad51 C	31515
SUM159 Cas9 Blast	1067
SUM159 Rad51 D	35935

Courbes de régression non linéaires de la viabilité cellulaire en réponse au Ola

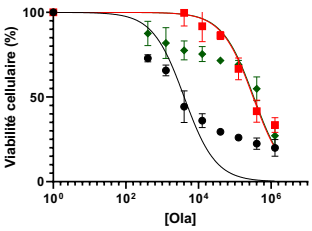

	IC50 (nM)
UWB1	4015
UWB1+B1	316107
UWB1 R	331330

Courbes de régression non linéaires de la viabilité cellulaire en réponse à l'Olaparib

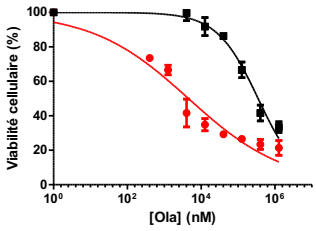

	IC50 (nM)
UWB1	4524
UWB1+B1	347825

CDDP mono

Courbes de régression non linéaires de la viabilité cellulaire en réponse au CDDP

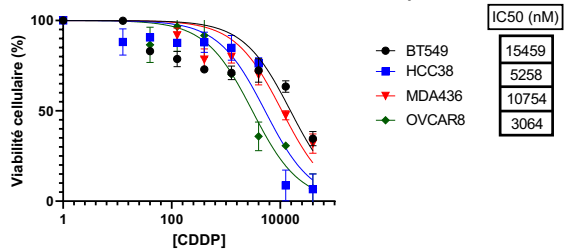

Courbes de régression non linéaires de la viabilité cellulaire en réponse au CDDP

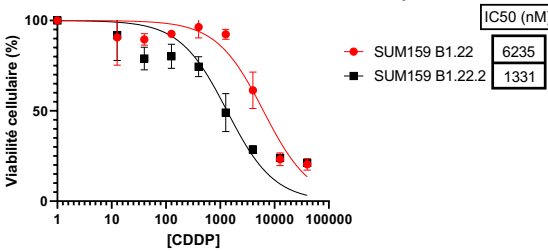

Courbes de régression non linéaires de la viabilité cellulaire en réponse au CDDP

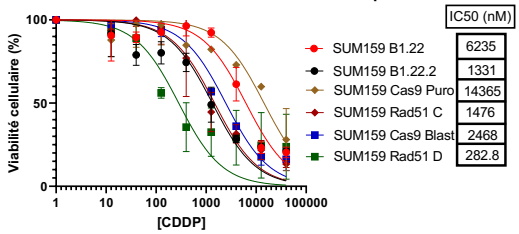

Courbes de régression non linéaires de la viabilité cellulaire en réponse au CDDP

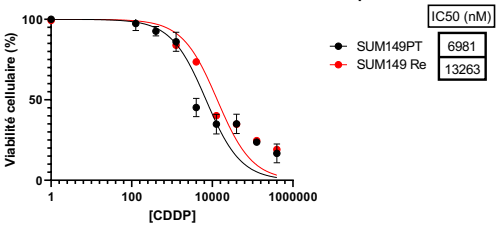

Courbes de régression non linéaires de la viabilité cellulaire en réponse au CDDP

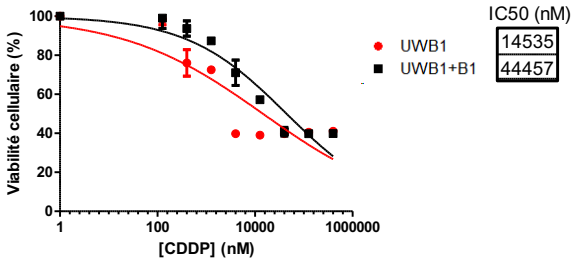

Courbes de régression non linéaires de la viabilité cellulaire en réponse au CDDP

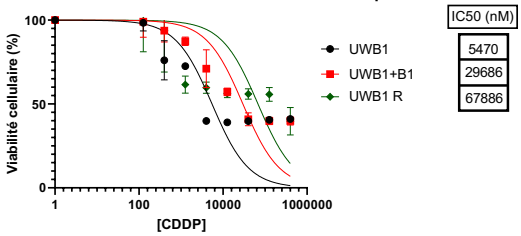

Gemcitabine mono

Courbes de régression non linéaires de la viabilité cellulaire en réponse à la gemcitabine

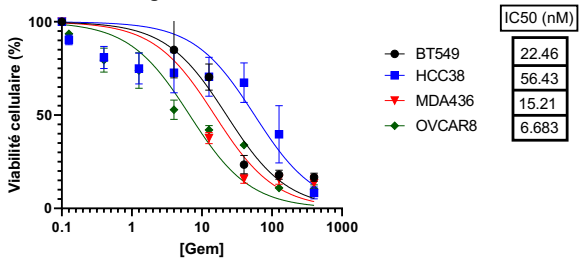

Courbes de régression non linéaires de la viabilité cellulaire en réponse à la gemcitabine (n=1)

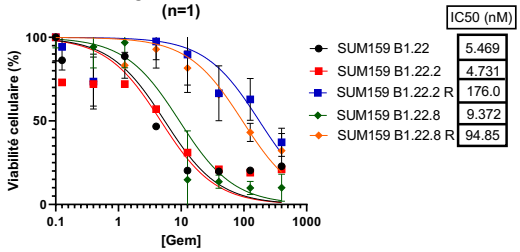

Courbes de régression non linéaires de la viabilité cellulaire en réponse à la gemcitabine

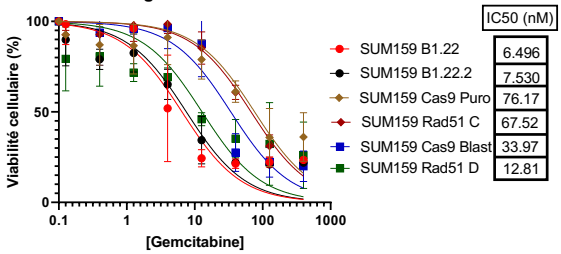

Courbes de régression non linéaires de la viabilité cellulaire en réponse à la gemcitabine

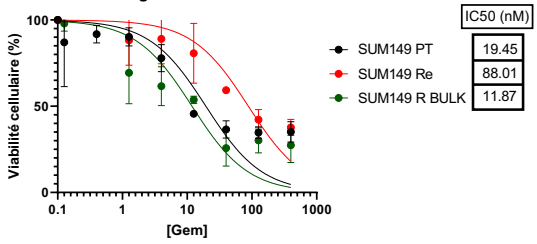

Courbes de régression non linéaires de la viabilité cellulaire en réponse à la Gemcitabine

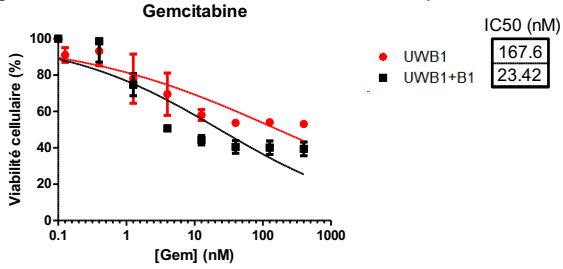

Courbes de régression non linéaires de la viabilité cellulaire en réponse à la gemcitabine

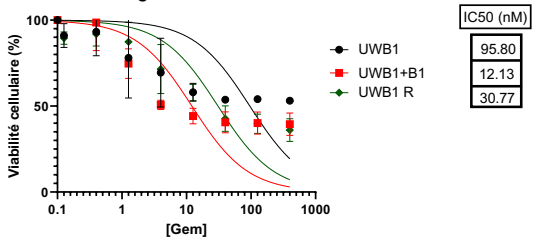

Dinaciclib mono

Courbes de régression non linéaires de la viabilité cellulaire en réponse au dinaciclib (CDKi)

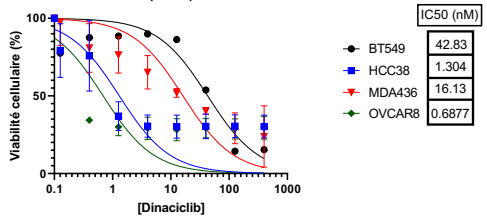

	IC50 (nM)
BT549	42.83
HCC38	1.304
MDA436	16.13
OVCAR8	0.6877

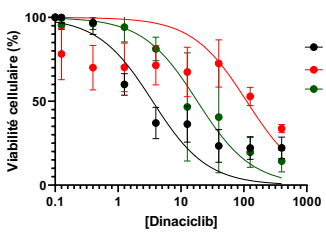

	IC50 (nM)
SUM149PT	3.542
SUM149 Re	111.1
SUM149 R BULK	18.22

Courbes de régression non linéaires de la viabilité cellulaire en réponse au Dinaciclib (CDKi)

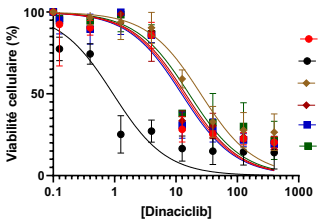

	IC50 (nM)
SUM159 B1.22	13.25
SUM159 B1.22.2	0.9434
SUM159 Cas9 Puro	25.30
SUM159 Rad51 C	14.26
SUM159 Cas9 Blast	12.36
SUM159 Rad51 D	16.33

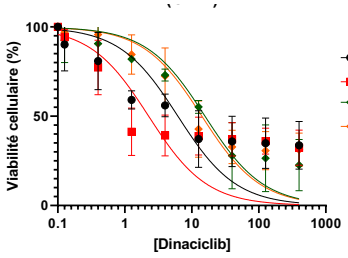

	IC50 (nM)
UWB1	6.204
UWB1+B1	2.272
UWB1 R	15.74
UWB1 Rb	14.15

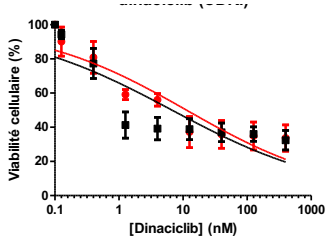

	IC50 (nM)
UWB1	11.35
UWB1+B1	6.733

SR-4835 mono

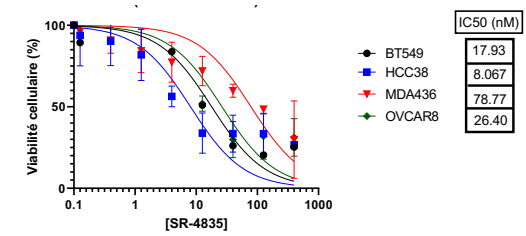
Viabilité cellulaire (%)
100
50
0
0.1
1
10
100
1000
[SR-4835]
IC50 (nM)
BT549 17.93
HCC38 8.067
MDA436 78.77
OVCAR8 26.40

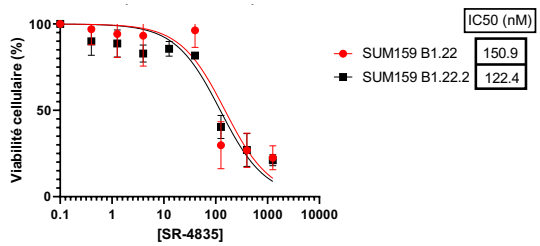
Viabilité cellulaire (%)
100
50
0
0.1
1
10
100
1000
10000
[SR-4835]
IC50 (nM)
SUM159 B1.22 150.9
SUM159 B1.22.2 122.4

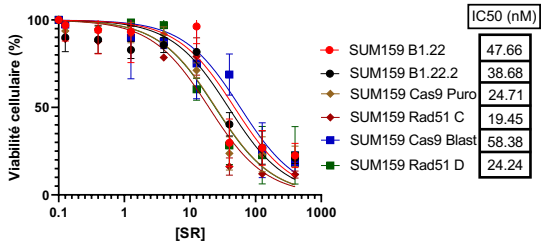
Viabilité cellulaire (%)
100
50
0
0.1
1
10
100
1000
[SR]
IC50 (nM)
SUM159 B1.22 47.66
SUM159 B1.22.2 38.68
SUM159 Cas9 Puro 24.71
SUM159 Rad51 C 19.45
SUM159 Cas9 Blast 58.38
SUM159 Rad51 D 24.24

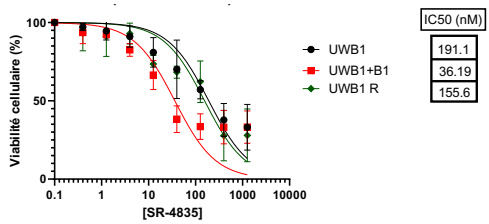
Viabilité cellulaire (%)
100
50
0
0.1
1
10
100
1000
10000
[SR-4835]
IC50 (nM)
UWB1 191.1
UWB1+B1 36.19
UWB1 R 155.6

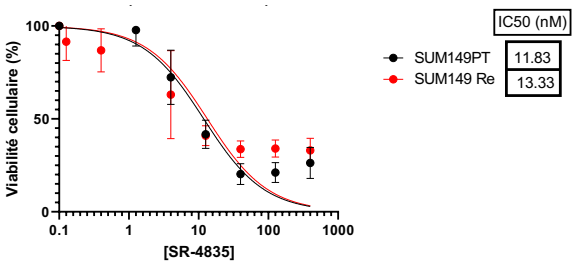
Viabilité cellulaire (%)
100
50
0
0.1
1
10
100
1000
[SR-4835]
IC50 (nM)
SUM149PT 11.83
SUM149 Re 13.33

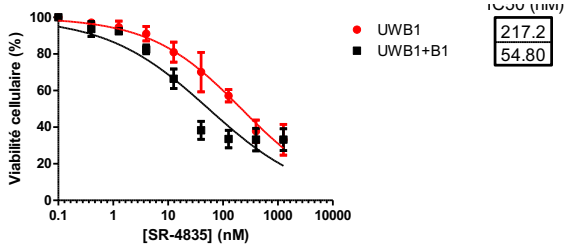
Viabilité cellulaire (%)
100
80
60
40
20
0
0.1
1
10
100
1000
10000
[SR-4835] (nM)
UWB1 217.2
UWB1+B1 54.80

Olaparib + Dinaciclib combo

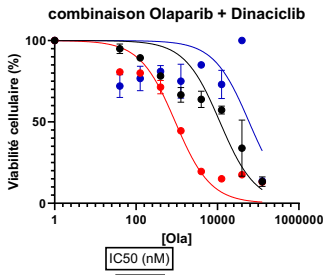

	IC50 (nM)
SUM159 WT	11481
SUM159 WT Ola+Dina 1nM	921.0
SUM159 WT Ola+Dina 10nM	59810

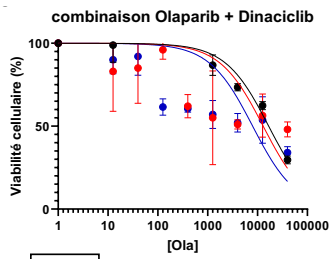

	IC50 (nM)
BT549 IC50 Ola	16741
BT549 Ola+Dina 1nM	12998
BT549 Ola+Dina 10nM	7990

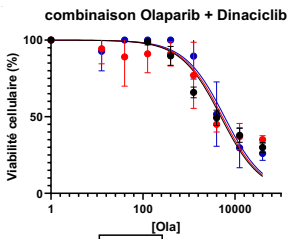

	IC50 (nM)
MDA436	4928
MDA436 Ola+Dina 1nM	5325
MDA436 Ola+Dina 10nM	5916

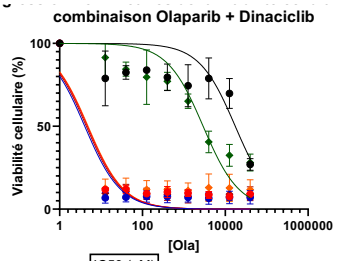

	IC50 (nM)
SUM159 B1.22	17457
SUM159 B1.22 Ola+Dina 1nM	4.687
SUM159 B1.22 Ola+Dina 10nM	4.043
SUM159 B1.22.2	2922
SUM159 B1.22.2 Ola+Dina 1nM	4.856
SUM159 B1.22.2 Ola+Dina 10nM	4.415

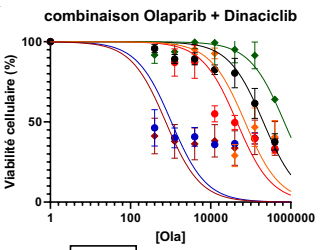

	IC50 (nM)
SUM149 PT	205438
SUM149 PT Ola+Dina 1nM	45074
SUM149 PT Ola+Dina 10nM	1046
SUM149 Re	682569
SUM149 Re Ola+Dina 1nM	71847
SUM149 Re Ola+Dina 10nM	756.2

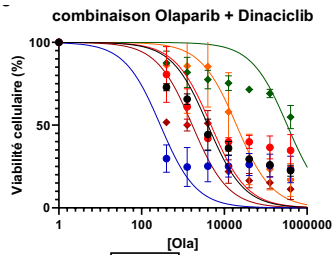

	IC50 (nM)
UWB1	4008
UWB1 PT Ola+Dina 1nM	4767
UWB1 PT Ola+Dina 10nM	284.0
UWB1 R BULK	330692
UWB1 R BULK Ola+Dina 1nM	19688
UWB1 R BULK Ola+Dina 10nM	1679

Olaparib + SR-4835 combo

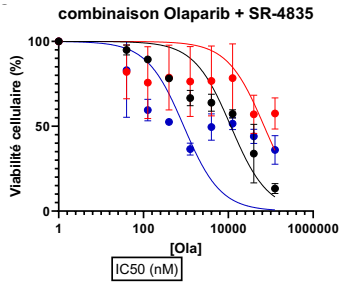

	IC50 (nM)
SUM159 WT	11481
SUM159 WT Ola+SR 1nM	70165
SUM159 WT Ola+SR 10nM	892.5

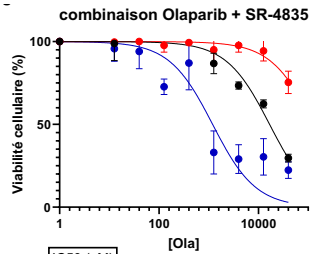

	IC50 (nM)
BT549	16741
BT549 Ola+SR 1nM	Non atteint
BT549 Ola+SR 10nM	1197

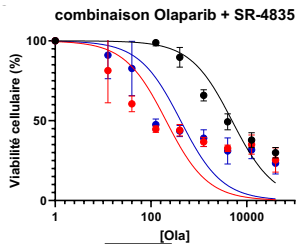

	IC50 (nM)
MDA436	4928
MDA436 Ola+SR 1nM	206.8
MDA436 Ola+SR 10nM	417.0

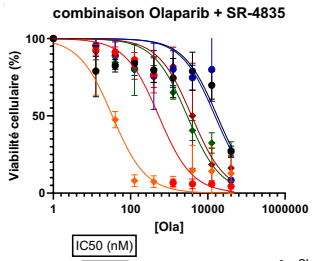

	IC50 (nM)
SUM159 B1.22	17457
SUM159 B1.22 Ola+SR 1nM	535.1
SUM159 B1.22 Ola+SR 10nM	15315
SUM159 B1.22.2	2922
SUM159 B1.22.2 Ola+SR 1nM	33.69
SUM159 B1.22.2 Ola+SR 10nM	3812

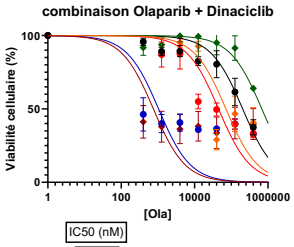

	IC50 (nM)
SUM149 PT	205438
SUM149 PT Ola+Dina 1nM	45074
SUM149 PT Ola+Dina 10nM	1046
SUM149 Re	682569
SUM149 Re Ola+Dina 1nM	71847
SUM149 Re Ola+Dina 10nM	756.2

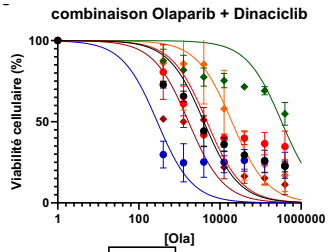

	IC50 (nM)
UWB1	4008
UWB1 PT Ola+Dina 1nM	4767
UWB1 PT Ola+Dina 10nM	284.0
UWB1 R BULK	330692
UWB1 R BULK Ola+Dina 1nM	19688
UWB1 R BULK Ola+Dina 10nM	1679

CDDP + Dinaciclib combo

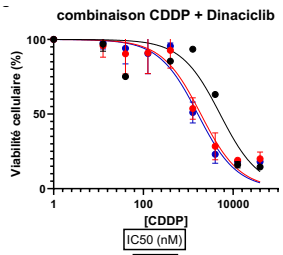

	IC50 (nM)
SUM159 WT	5124
SUM159 WT CDDP+Dina 1nM	1907
SUM159 WT CDDP+Dina 10nM	1635

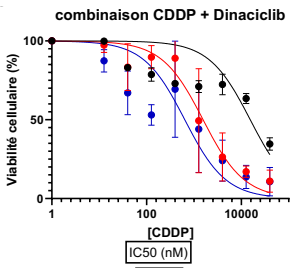

	IC50 (nM)
BT549	15427
BT549 CDDP+Dina 1nM	1559
BT549 CDDP+Dina 10nM	640.5

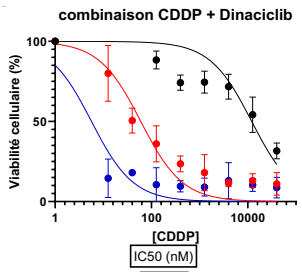

	IC50 (nM)
MDA436	12077
MDA436 CDDP+Dina 1nM	60.18
MDA436 CDDP+Dina 10nM	5.704

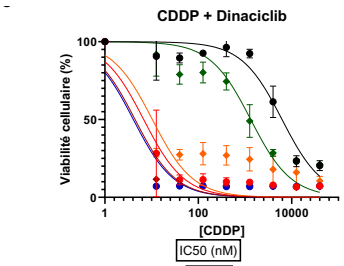

	IC50 (nM)
SUM159 B1.22	6221
SUM159 B1.22 CDDP+Dina 1nM	6.780
SUM159 B1.22 CDDP+Dina 10nM	4.065
SUM159 B1.22.2	1328
SUM159 B1.22.2 CDDP+Dina 1nM	10.40
SUM159 B1.22.2 CDDP+Dina 10nM	4.434

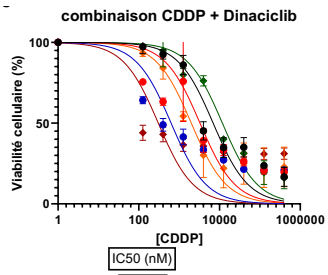

	IC50 (nM)
SUM149PT	6964
SUM149 PT CDDP+Dina 1nM	3287
SUM149 PT CDDP+Dina 10nM	633.4
SUM149 Re	11806
SUM149 Re CDDP+Dina 1nM	2003
SUM149 Re CDDP+Dina 10nM	304.7

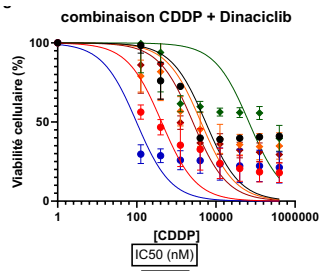

	IC50 (nM)
UWB1	5291
UWB1 PT CDDP+Dina 1nM	423.2
UWB1 PT CDDP+Dina 10nM	98.37
UWB1 R BULK	67886
UWB1 R BULK CDDP+Dina 1nM	4178
UWB1 R BULK CDDP+Dina 10nM	2608

CDDP + SR-4835 combo

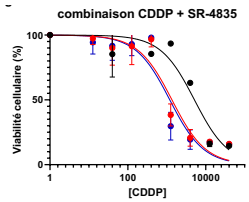

	IC50 (nM)
SUM159 WT	5138
SUM159 WT CDDP+SR 1nM	1360
SUM159 WT CDDP+SR 10nM	1195

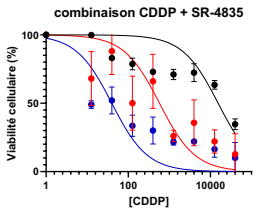

	IC50 (nM)
BT549	15427
BT549 CDDP+SR 1nM	576.2
BT549 CDDP+SR 10nM	39.78

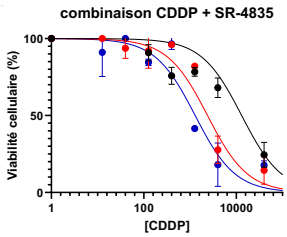

	IC50 (nM)
MDA436	13083
MDA436 CDDP+SR 1nM	2387
MDA436 CDDP+SR 10nM	1291

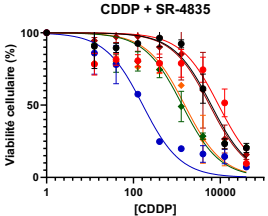

	IC50 (nM)
SUM159 B1.22	6221
SUM159 B1.22 CDDP+SR 1nM	9151
SUM159 B1.22 CDDP+SR 10nM	164.6
SUM159 B1.22.2	1328
SUM159 B1.22.2 CDDP+SR 1nM	1521
SUM159 B1.22.2 CDDP+SR 10nM	5705

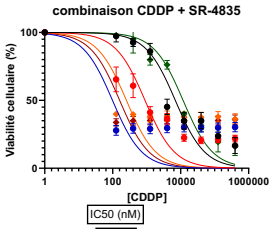

	IC50 (nM)
SUM149 PT	6964
SUM149 PT CDDP+SR 1nM	894.7
SUM149 PT CDDP+SR 10nM	98.74
SUM149 Re	11806
SUM149 Re CDDP+SR 1nM	253.7
SUM149 Re CDDP+SR 10nM	160.3

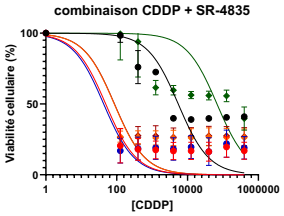

	IC50 (nM)
UWB1	5291
UWB1 PT CDDP+SR 1nM	48.95
UWB1 PT CDDP+SR 10nM	42.89
UWB1 R BULK	67886
UWB1 R BULK CDDP+SR 1nM	85.18
UWB1 R BULK CDDP+SR 10nM	86.75

Gemcitabine combo

Courbes de régression non linéaires de la viabilité cellulaire en réponse à la combinaison Gemcitabine + Dinaciclib

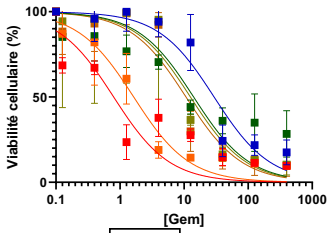

	IC50 (nM)
SUM159 BLAST	29.43
SUM159 BLAST Gem+Dina 1nM	0.7961
SUM159 BLAST Gem+Dina 10nM	1.636
SUM159 Rad51 D	14.10
SUM159 Rad51D Gem+Dina 1nM	12.56
SUM159 Rad51D Gem+Dina 10nM	10.72

Courbes de régression non linéaires de la viabilité cellulaire en réponse à la combinaison Gemcitabine + Dinacilib

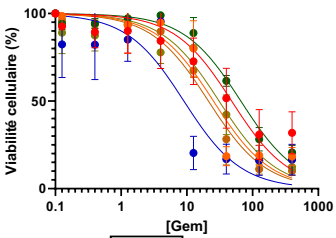

	IC50 (nM)
SUM159 PURO	48.12
SUM159 PURO Gem+Dina 1nM	25.44
SUM159 PURO Gem+Dina 10nM	9.028
SUM159 Rad51 C	66.36
SUM159 Rad51C Gem+Dina 1nM	30.94
SUM159 Rad51C Gem+Dina 10nM	21.33

Courbes de régression non linéaires de la viabilité cellulaire en réponse à la combinaison Gemcitabine + SR

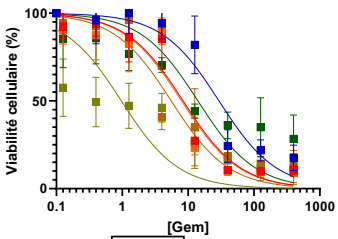

	IC50 (nM)
SUM159 BLAST	29.43
SUM159 Rad51D Gem+SR 1nM	8.407
SUM159 BLAST Gem+SR 10nM	7.981
SUM159 Rad51 D	14.10
SUM159 Rad51D Gem+SR 1nM	0.9699
SUM159 Rad51D Gem+SR 10nM	5.541

Courbes de régression non linéaires de la viabilité cellulaire en réponse à la combinaison Gemcitabine + SR-4835

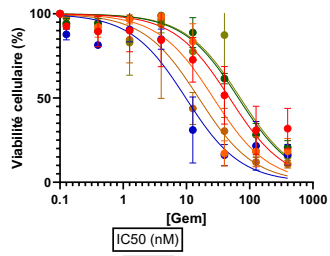

	IC50 (nM)
SUM159 PURO	48.12
SUM159 PURO Gem+SR 1nM	26.72
SUM159 PURO Gem+SR 10nM	9.793
SUM159 Rad51 C	66.36
SUM159 Rad51C Gem+Dina 1nM	71.31
SUM159 Rad51C Gem+Dina 10nM	15.67